2023 | JANUARY - DECEMBER 5th YEAR 1st EDITION

IJIET

INTERNATIONAL JOURNAL OF INDUSTRIAL EDUCATION AND TECHNOLOGY

ISSN 2673-0448 (Print)

SCHOOL OF INDUSTRIAL EDUCATION AND TECHNOLOGY
KING MONGKUT'S INSTITUTE OF TECHNOLOGY LADKRABANG

International Journal of Industrial Education and Technology
ISSN 2673-0448
Vol. 5 No. 1 (January–December) 2023

Assoc. Prof. Dr. Tuanjai Archevapanich	Rajamangala University of Technology Suvarnabhumi, Nonthaburi
Assoc. Prof. Dr. Udomvit Chaisakulkiet	Rajamangala University of Technology Rattanakosin
Assoc. Prof. Attarporn Ridhikerd	(Retired civil servant)
	Anusawari sub-district, Bang Khen district, Bangkok
Asst. Prof. Dr. Anusit Anmanatarkul	King Mongkut's University of Technology Thonburi
Asst. Prof. Dr. Janpanit Surasin	Burapha University
Asst. Prof. Dr. Pattama Pattanapong	Mahidol University
Asst. Prof. Dr. Petcharat Suriyachai	Prince of Songkla University
Asst. Prof. Dr. Sasitorn Suwannathep	King Mongkut's University of Technology Thonburi
Asst. Prof. Dr. Suchada Katdee	Rajamangala University of Technology Phra Nakhon
Asst. Prof. Dr. Suebpong Prabyai	Ramkhamhaeng University
Asst. Prof. Dr. Thosporn Sangsawang	Rajamangala University of Technology Thanyaburi
Asst. Prof. Dr. Yupin Phasuk	Khon Kaen University
Asst. Prof. Pramote Anunvarapong	Rajamangala University of Technology Krungthep
Dr. Bundit Prasantree	Phranakhon Rajabhat University
Dr. Kiattisak Siphimanwat	National Electronics and Computer Technology Center
Dr. Pakorn Prajuabwan	Kanchanaburi Rajabhat University
Dr. Saowalak Saengkae	Rajamangala University of Technology Krungthep
Dr. Somjai Klin-Ngam	Phranakhon Rajabhat University University
Dr. Somporn Seewattanapon	Rajamangala University of Technology Suvarnabhumi

2.3 Internal Editor Board Committees (King Mongkut's Institute of Technology Ladkrabang)

Prof. Dr. Koompong Noobanjong
Prof. Dr. Pakkapong Poungsuk
Prof. Dr. Pornchai Supnithi
Assoc. Prof. Dr. Aukkapong Sukkamart
Assoc. Prof. Dr. Boonchan Sisan
Assoc. Prof. Dr. Chaturong Louhapensang
Assoc. Prof. Dr. Kanchana Boonpuck
Assoc. Prof. Dr. Kunya Tuntivisoottikul
Assoc. Prof. Dr. Paitoon Pimdee
Assoc. Prof. Dr. Pariyaporn Tungkunanan
Assoc. Prof. Dr. Pinmanee Kwanmuang
Assoc. Prof. Dr. Piya Supavarasuwat
Assoc. Prof. Dr. Ratchadakorn Phonpakdee
Assoc. Prof. Dr. Sirirat Petsangsri
Assoc. Prof. Dr. Somkiat Tuntiwongwanich
Assoc. Prof. Dr. Sompol Dumrongsatian
Assoc. Prof. Dr. Sunti Tuntrakool
Assoc. Prof. Dr. Suwanna Bengthong
Assoc. Prof. Dr. Thanin Ratanaolarn
Assoc. Prof. Dr. Winai Jaikla
Assoc. Prof. Dr. Wisuit Sunthonkanokpong

Asst. Prof. Dr. Apirath Limmanee
Asst. Prof. Dr. Jatuporn Anuchai
Asst. Prof. Dr. Pitsini Mano
Asst. Prof. Dr. Prasert Kenpankho
Asst. Prof. Dr. Sarawut Intorrathed
Asst. Prof. Dr. Somchai Maunsaiyat
Asst. Prof. Dr. Thanate Piromgarn
Asst. Prof. Nida Larpsrisawad
Dr. Pattanida Sodabun
Dr. Pattraporn Patthararangsarith
Dr. Ratree Siripant

3. Design and Approved Printing

(Thai Language Approval)

Asst. Prof. Dr. Ampapan Tuntinakhongul
Asst. Prof. Dr. Jatuporn Anuchai

(English Language Approval)

Asst. Prof. Dr. Ampapan Tuntinakhongul

Cover Design

Mr.Teeraphat Naegkhunthod

Information Technology

Assoc. Prof. Dr. Piya Supavarasuwat
Mr.Mai Charoentham
Mr.Prayoot Kunthong
Mrs.Jantanee Supsaendee

4. Membership Service

Mrs.Jantanee Supsaendee

5. Registration Service

Mrs.Jantanee Supsaendee

6. Assistant Editor

Mrs.Jantanee Supsaendee

Publishing: One issue per year
The 1st issue for January to December

Submission: Continuously

Scopes
To accept article which focus on industrial education, education and technology.

Selecting speculator for article Criteria
Criteria from speculators as follows:
- Article from individual inside institute is speculated by only speculators outside institute
- Article from individual outside institute is speculated by 1 speculator inside institute and 2 speculator outside institute

Website: https://www.tci-thaijo.org/index.php/IJIET

E-mail: journal.ided@kmitl.ac.th

Address: School of Industrial Education and Technology,
King Mongkut's Institute of Technology Ladkrabang
No.1, Soi Chalongkrung 1, Chalongkrung Road,
Ladkrabang, Bangkok, 10520
Tel: 08 6349 6020 or 02 329 8000 ext.3723
Fax: 02 329 8435

Comment, content, and language usages in the article regarding on author's responsibility

Editorial Statement

On behalf of the International Journal of Industrial Education and Technology (IJIET) editorial boards, I would like to sincerely thank you very much for your kind support. If you would like to give us comments and suggestions regarding on this issue, I would appreciate and accept that for making things better. As an editor in chief of IJIET, I would like to welcome and present you the third issue which is mainly to offer the research contents and articles in the fields of industrial education including education and technology. IJIET consists of three contents which are review article, book review, and research articles, respectively. For this IJIET issue, a review article is “GNSS PRECIPITABLE WATER VAPOR” and a book review is “THE SUN, THE EARTH, AND NEAR-EARTRH SPACE” including three research papers. I would like to invite you to read all interesting contents authored by a professional and intelligent group of writers who are volunteers to share their outcomes of research and professional discussions.

With best regards,

Assistant Professor Dr. Prasert Kenpankho, D.Eng.
Editor in Chief
International Journal of Industrial Education and Technology (IJIET)

Contents	Page

Review Article

GNSS PRECIPITABLE WATER VAPOR A1-A6

Rungsan Bangkuan, Chollada Pansong, and Supawit Nambut

Book Review

BOOK REVIEW: THE SUN, THE EARTH, AND NEAR-EARTRH SPACE AUTHOR: JOHN A. EADY B1-B6

Thanapon Keokhumcheng, Patiphan Sumniang, Supawit Nambut, and Chollada Pansong

Research Articles

COMPARISON OF SEVERE GEOMAGNETIC STORM EVENT AND LOW-LATITUDE TOTAL ELECTRON CONTENT ANOMALIES C1-C9

Wishapol Sittichai, Sunadda Koednawee, and Chollada Pansong

SKY PLOT VISIBILITY BASED ON BEIDOU AND GPS SATELLITES OVER BANGKOK, THAILAND C10-C19

Thanapon Keokhumcheng, Bussara Pasew, and Tawatchai Samosol

THE STUDY OF LOW-COST ROBOTICS PLATFORM FOR BEIDOU SATELLITES NAVIGATION SYSTEM C20-C28

Patiphan Sumniang, Chinakrid Janak, and Canjie Huang

IJIET
INTERNATIONAL JOURNAL
OF INDUSTRIAL EDUCATION AND TECHNOLOGY
ISSN 2673-0448

Review Article

GNSS PRECIPITABLE WATER VAPOR

Rungsan Bangkuan[1], Chollada Pansong[2], and Supawit Nambut[3]*
Email: 6503603@kmitl.ac.th[1], chollada_p@rmutt.ac.th[2], and supawit.nat@svit.ac.th[3]*

Received: December 12, 2023
Revised: December 15, 2023
Accepted: December 20, 2023

ABSTRACT

This review article centers on tropospheric delays in Global Navigation Satellite System (GNSS) positioning and the methodology for estimating Zenith Total Delay (ZTD), which encompasses Zenith Hydrostatic Delay (ZHD) and Zenith Wet Delay (ZWD). The precise modeling and estimation of these delays are paramount for achieving high-precision GNSS positioning and valuable tools for tropospheric monitoring. The process of GNSS Precipitable Water Vapor (PWV) retrieval entails the calculation of ZWD by subtracting ZHD from ZTD. The Weighted Mean Temperature (Tm) stands out as a crucial parameter influencing the calculations of GNSS PWV, and the accuracy of GNSS PWV hinges on the precision of both Tm and ZHD.

Keywords: Precipitable water vapor, GNSS, ZTD, ZHD, ZWD

*Corresponding author E-mail: Supawit.nat@svit.ac.th
[1] Department of Enginering Education, School of Industrial Education and Technology, King Mongkut's Institute of Technology Ladkrabang, Bangkok, 10520 Thailand
[2] Department of Technical Education, Faculty of Technical Education, Rajamangala University of Technology Thanyaburi, Pathum Thani, 12110 Thailand
[3*]Management of Digital Innovation for Business School of Business Administration, Suvarnabhumi Institute of Technology, Samut Prakarn, 10540 Thailand

I. INTRODUCTION

Water vapor plays a crucial role in Earth's atmospheric processes, influencing weather patterns and contributing to the overall climate system. Accurate measurement and monitoring of atmospheric water vapor content are essential for understanding weather dynamics, climate variability, and improving weather forecasting capabilities. One advanced technique for obtaining precise information about water vapor in the atmosphere is through the use of Global Navigation Satellite System (GNSS) technology.

GNSS, encompassing satellite constellations such as Global Positioning System (GPS), GLObalnaya NAvigatsionnaya Sputnikovaya Sistema (GLONASS), Galileo, BeiDou Navigation Satellite System (BeiDou), Quasi-Zenith Satellite System (QZSS), and Indian Regional Navigation Satellite System (IRNSS), has evolved beyond its primary role in navigation to become a valuable tool in atmospheric science. One significant application is the estimation of Precipitable Water Vapor (PWV), a key parameter characterizing the amount of water vapor present in the troposphere. The fundamental principle underlying GNSS PWV estimation lies in the analysis of signal delays experienced by GNSS signals as they traverse the Earth's atmosphere. When GNSS signals pass through the troposphere, they encounter delays due to atmospheric conditions, with water vapor being a major contributor to these delays. Leveraging the dual-frequency signals transmitted by GNSS satellites, researchers can differentiate and quantify the tropospheric delay associated with water vapor.

The process involves calculating the Zenith Total Delay (ZTD), which represents the total delay experienced by GNSS signals from the satellite to the receiver, including contributions from water vapor. By employing mathematical models and algorithms, scientists can separate the dry component of the atmosphere and isolate the water vapor-related delay. Furthermore, a mapping function is applied to account for variations in the atmosphere's refractivity, ensuring accurate corrections. The final result is a precise estimation of the Integrated Water Vapor (IWV), which represents the total amount of water vapor along the vertical column above a specific location. The capability to continuously monitor GNSS signals allows for real-time tracking of changes in atmospheric water vapor content. This information proves invaluable in various fields, including meteorology, climate research, and environmental monitoring. GNSS-derived PWV data contribute to improving weather forecasts, understanding climate patterns, and enhancing our ability to respond to and mitigate the impacts of extreme weather events (Bevis et al.,1992, pp. 15787-15801; Domingo & Macalalad, 2022, pp. 1-13; Han et al., 2023, pp. 1-14; Huang et al., 2021, pp. 1-18).

In this review, the integration of GNSS technology into atmospheric studies represents a remarkable advancement, offering a non-intrusive and globally accessible means to observe and quantify one of the most influential components of Earth's atmosphere – water vapor. As researchers continue to refine GNSS-based techniques, the potential for enhanced understanding and prediction of atmospheric phenomena continues to grow, ushering in new possibilities for scientific inquiry and practical applications.

II. WATER VAPOR

Water vapor is the gaseous form of water and is an essential component of Earth's atmosphere. It plays a crucial role in the planet's weather and climate systems. Understanding the principles of water vapor involves recognizing its unique properties and the processes that govern its presence in the atmosphere.

Phase transition: Water exists in three primary phases-solid (ice), liquid (water), and gas (water vapor). The transition between these phases is governed by temperature and pressure. When water absorbs heat, it undergoes a phase transition from liquid to vapor, a process known as evaporation.

Evaporation and condensation: Evaporation is the process by which water molecules gain enough energy to break their bonds and become vapor. This occurs primarily at the surface of bodies of water, such as oceans, lakes, and rivers. Conversely, condensation is the process where water vapor loses energy and transitions back to liquid form, forming clouds and precipitation.

Water vapor in the atmosphere: Water vapor is present in varying concentrations in the Earth's atmosphere. It is most abundant in the troposphere, the lowest layer of the atmosphere, where weather events occur. The amount of water vapor the air can hold depends on its temperature; warmer air can hold more water vapor than cooler air.

Role in the water cycle: Water vapor is a central player in the Earth's water cycle. As the sun heats the Earth's surface, water evaporates into the atmosphere. Once in the atmosphere, water vapor can be transported over great distances by atmospheric currents. When conditions are right, it can condense to form clouds and participate in precipitation events.

Greenhouse gas: Water vapor is also a significant greenhouse gas, contributing to the natural greenhouse effect. While carbon dioxide and other greenhouse gases are often discussed in the context of climate change, water vapor's role is critical. It amplifies the warming effect by increasing as the atmosphere warms, creating a feedback loop.

Humidity: Humidity is a measure of the amount of water vapor present in the air. It can be expressed as absolute humidity (the actual amount of water vapor per unit volume of air) or relative humidity (the percentage of water vapor present compared to the maximum amount the air could hold at a given temperature).

III. GNSS PRECIPITABLE WATER VAPOR

Tropospheric delays are commonly recognized as a primary source of errors in GNSS positioning, and as such, they are typically modeled and estimated in the GNSS analysis process. The estimation of these delays not only enables high-precision GNSS positioning but also serves as a valuable tool for tropospheric monitoring. Traditionally, the zenith total delay (ZTD) comprises two components: the zenith hydrostatic delay (ZHD) and the zenith wet delay (ZWD). These components are linked to individual satellite observations and their associated slant delays through specific mapping functions. The ZTD depends on the hydrostatic (Air pressure-related) part and, crucially, on the partial water vapor pressure in the lower atmosphere. By estimating the wet component of the delay (i.e., the ZWD), GNSS observations provide a direct means to observe the quantity of atmospheric water vapor. This water vapor is an active and abundant component of the climate system.

A. Methodology

As GNSS signals traverse the lower atmosphere, they encounter the atmospheric delay effect, resulting in a decrease in signal propagation speed and the bending of the signal path-a phenomenon commonly referred to as atmospheric delay. This delay predominantly occurs in the troposphere and is specifically known as tropospheric delay. The delay amount in the zenith direction is termed zenith total delay (ZTD), which comprises two primary components: zenith hydrostatic delay (ZHD) and zenith wet delay (ZWD). In GNSS data processing, accurate estimation of ZTD is achievable, with ZHD calculated primarily using the Saastamoinen model based on station latitude and surface pressure or derived from numerical weather models (NWM). ZWD, essential for GNSS meteorology, is computed by subtracting ZHD from ZTD.

In the realm of GNSS meteorology, the weighted mean temperature (Tm) assumes a critical role as a parameter for computing GNSS Precipitable Water Vapor (PWV). PWV is a significant factor influencing the calculation of high-precision PWV values. Consequently, the accuracy of GNSS PWV is heavily contingent on the precision of both Tm and ZHD (Huang et al., 2021, pp. 1-18).

Domingo and Macalalad (2022, pp. 1-13) studied on temporal analysis of GNSS-based precipitable water vapor during rainy days over the Philippines from 2015 to 2017. They employed a globally accepted model, the Tm model by Bevis, as shown in Figure 1.

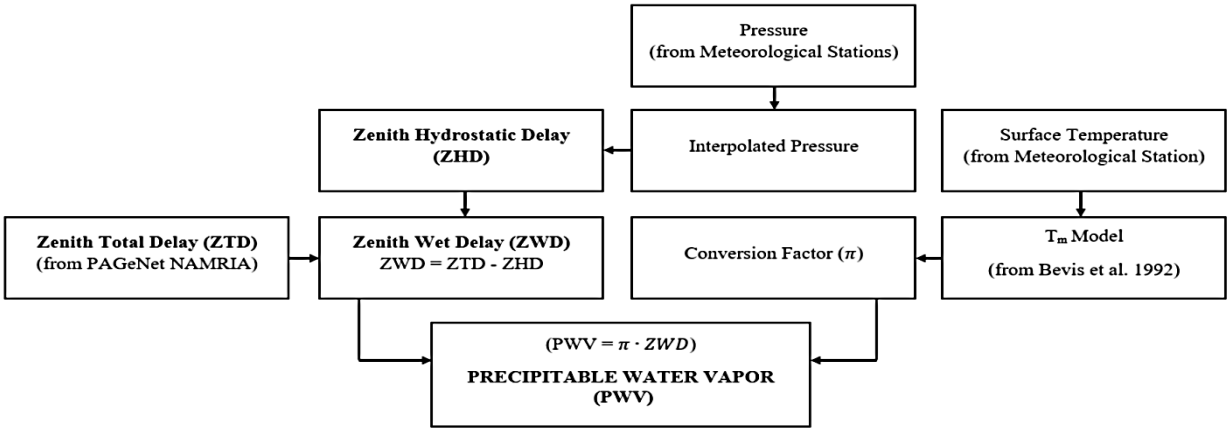

Figure 1 Flow chart for obtaining GNSS PWV
Source: Domingo and Macalalad (2022, p. 4)

B. Equations

Bevis et al. (1992, pp. 15787-15801) introduced the concept of GPS meteorology, wherein ZTD is obtained from GNSS observations. ZHD is typically estimated using the Saastamoinen model based on surface pressure measurements or derived from Numerical Weather Models (NWM). Subsequently, the ZWD value is determined by subtracting ZHD from ZTD (Domingo & Macalalad, 2022, pp. 3-4; Han et al., 2023, pp. 3-4; Huang et al., 2021, pp. 3-7).

The procedure for GNSS PWV calculating is outlined as follows:

$$\mathrm{ZWD} = \mathrm{ZTD} - \mathrm{ZHD} \tag{1}$$

$$\Pi = \frac{10^6}{\rho_w R_v \left[\frac{k_3}{T_m} + k'_2\right]} \tag{2}$$

$$\mathrm{PWV} = \Pi \,.\, \mathrm{ZWD} \tag{3}$$

where Π is the dimensionless atmospheric water vapor conversion factor, ρ_w is the density of liquid water, R_v represents the universal gas constant for water vapor, and k'_2 and k_3 are atmospheric physical constants.

The weighted mean temperature (Tm) can be calculated using the equation as:

$$T_m = \frac{\int \left(\frac{e}{T}\right) dH}{\int \left(\frac{e}{T^2}\right) dH} \quad (4)$$

where e indicates the water vapor pressure, T refers to the corresponding temperature, and dH indicates the atmosphere thickness.

The Vertical correction investigation for ZHD, the vertical adjustment holds significant importance in the development of tropospheric delay and Tm models. Numerous successful investigations have emphasized that the precision of the correction model significantly influences the accuracy of high-precision positioning. Crétaux et al. (2009, pp. 723–735) identified various challenges associated with these corrections, particularly in the context of dry tropospheric corrections. Previous research has indicated that the vertical adjustment of ZHD can be accomplished by considering the height dependence of atmospheric pressure, as utilized by Kouba 2008 (Huang et al., 2021, pp. 3-7), expressed as:

$$P_s = P_0[1 - 0.0000226 \,.\, (h_s - h_0)]^{5.225} \quad (5)$$

$$\mathrm{ZHD} = \frac{0.0022768 \,.\, P_s}{1 - 0.0000226 \cos(2\varphi) - 0.28.10^{-6} .\, h_s} \quad (6)$$

where P_s and P_0 are the atmospheric surface pressures (in hPa) at heights h_s and h_0 (in m), φ is the geodetic latitude, and ZHD results in meters. The P_0 is obtained from GPT2w.

$$\mathrm{ZHD} = \mathrm{ZHD_{grid}} + 0.0022768 \,.\left(\frac{g \,.\, P_{grid}}{R \,.\, T_{grid}}\right).\,(h - h_{grid}) \quad (7)$$

where g is the gravity acceleration (9.8 m s^{-2}), and R is the gas constant (8.314 JK^{-1} mol^{-1}). p_{grid} and T_{grid} have been extracted from the new GPT2w model.

IV. RESULT REVIEW

GNSS signals passing through the lower atmosphere experience tropospheric delays, primarily due to atmospheric water vapor. Tropospheric delays, specifically ZTD, are modeled and estimated to enable high-precision GNSS positioning and tropospheric monitoring. ZTD consists of two main components: ZHD and ZWD. ZHD is traditionally estimated using models like the Saastamoinen model based on surface pressure or derived from Numerical Weather Models (NWM). ZWD is then obtained by subtracting ZHD from ZTD. PWV is calculated as the product of the atmospheric water vapor conversion factor (Π) and ZWD: PWV=Π·ZWD. Tm is a critical parameter influencing PWV calculations. Tm is determined by integrating water vapor pressure (e) over temperature (T) and its square over the atmosphere's thickness (dH).

V. CONCLUSION AND DISCUSSION

This review focuses on tropospheric delays GNSS positioning and the methodology for estimating ZTD, comprising ZHD and ZWD. The accurate modeling and estimation of these delays are crucial for high-precision GNSS positioning and serve as valuable tools for tropospheric monitoring. The procedure for GNSS PWV retrieval involves calculating ZWD by subtracting ZHD from ZTD. The weighted mean temperature (Tm) is a critical parameter influencing GNSS PWV calculations. The accuracy of GNSS PWV is contingent on the precision of both Tm and ZHD. Equations are provided for calculating ZWD, PWV, and Tm, with a focus on the vertical adjustment of ZHD. The height dependence of atmospheric pressure is considered, and a correction model is presented, emphasizing its importance in high-precision positioning. Temporal analyses of GNSS-based PWV during specific periods may be conducted to understand variations. Globally accepted models, such as the Tm model by Bevis, can be employed for comprehensive temporal studies. Vertical adjustment for ZHD, precision in the vertical adjustment of ZHD significantly influences high-precision positioning. Challenges, particularly in dry tropospheric corrections, are acknowledged. Vertical adjustment methods, considering the height dependence of atmospheric pressure, are proposed for accurate ZHD estimation.

AKNOWLEDGEMENT

We would like to thank Assistant Professor Dr. Prasert Kenpankho from Space, Satellite, and Study Laboratory (SSS Lab), Department of Engineering Education, King Mongkut's Institute of Technology Ladkrabang, Thailand for consulting on this review article.

REFERENCES

Bevis, M., Businger, S., Herring, T. A., Rocken, C., Anthes, R. A., & Ware, R. H. (1992). GPS meteorology: Remote sensing of atmospheric water vapor using the global positioning system. *Journal of Geophysical Research: Atmospheres, 97*(D14), 15787-15801.

Crétaux, J. F., Calmant, S., Romanovski, V., Shabunin, A., Lyard, F., Bergé-Nguyen, M., Cazenave, A., Hernandez, F., & Perosanz, F. (2009). An absolute calibration site for radar altimeters in the continental domain: Lake Issykkul in Central Asia. *Journal of Geodesy*, *83*(8), 723-735.

Domingo, A. L. S., & Macalalad, E. P. (2022). Temporal analysis of GNSS-based precipitable water vapor during rainy days over the Philippines from 2015 to 2017. *Atmosphere, 13*(3), 1-13.

Han, S., Liu, X., Jin, X., Zhang, F., Zhou, M., & Guo, J. (2023). Variations of precipitable water vapor in sandstorm season determined from GNSS data: The case of China's Wuhai. *Earth, Planets and Space*, *75*(12), 1-14.

Huang, L., Peng, H., Liu, L., Xiong, S., Xie, S., Chen, J., Li, J., & He, H. (2021). GNSS precipitable water vapor retrieval with the aid of NWM data for China. *Earth and Space Science, 8*, 1-18.

IJIET
INTERNATIONAL JOURNAL
OF INDUSTRIAL EDUCATION AND TECHNOLOGY
ISSN 2673-0448

Book Review

BOOK REVIEW: THE SUN, THE EARTH, AND NEAR-EARTH SPACE AUTHOR: JOHN A. EDDY

Thanapon Keokhumcheng[2*], Patiphan Sumniang[1], Supawit Nambut[3], and Chollada Pansong[4]
E-mail: kpongthanaponok@gmail.com[2*], patiphan.su@kmitl.ac.th[1], supawit.nat@svit.ac.th[3], and chollada_p@rmutt.ac.th[4]

Received: December 12, 2023
Revised: December 14, 2023
Accepted: December 20, 2023

ABSTRACT

We have completed reading "THE SUN, THE EARTH, AND NEAR-EARTH SPACE : A GUIDE TO THE SUN-EARTH SYSTEM" by John A. Eddy, utilizing it to comprehend the sun's impact on the world and life on Earth, and encompassing various global environments. This book has provided insights into radiation's influence on living organisms and diverse human activities such as communication, aviation, and positioning. We have gained knowledge that sunlight reaching Earth generates a magnetic field, directly impacting our planet. Upon reading, we observed that the content of this book aligns with the subject of our research. We are currently exploring the impact of solar-induced electron quantity in the atmosphere on communications systems and applications. We highly recommend this book for those interested in or studying satellite communications and space, as it proves to be both valuable and captivating.

Keywords: The Sun, The Earth, Near-Earth space

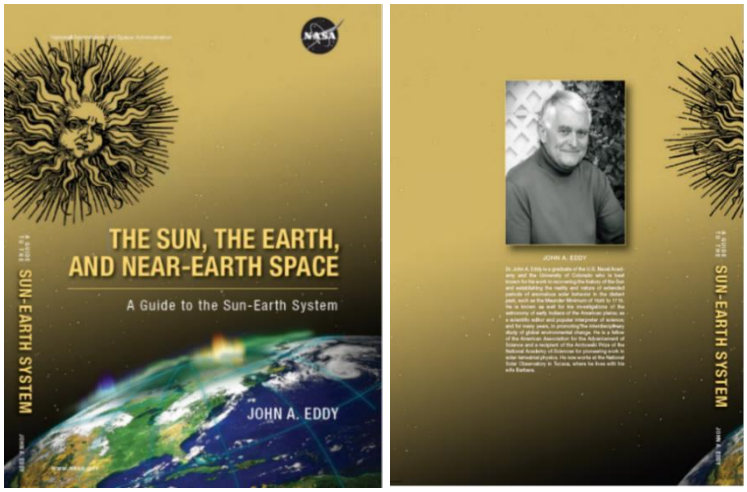

*Corresponding author E-mail: kpongthanaponok@gmail.com
[1*]Department of Engineering Education School of Industrial Education and Technology, King Mongkut's Institute of Technology Ladkrabang, Bangkok, 10520 Thailand
[2]Department of Electronics, Nongbualumphu Technical College, Nong Bua Lam Phu, 39000 Thailand
[3]Management of Digital Innovation for Business, School of Business Administration, Suvarnabhumi Institute of Technology, Samut Prakarn, 10540 Thailand
[4]Department of Technical Education, Faculty of Technical Education, Rajamangala University of Technology Thanyaburi, Pathum Thani, 12110 Thailand

The Earth is bathed in warmth by the sun, as it receives light from our closest star. Visible constellations emerge through the interaction of sunlight. Positioned over a million kilometers away, our galaxy, the Sun, comprises vast space, primarily composed of approximately 30 hydrogen and helium atoms per cubic foot. This cosmic expanse includes atoms, molecules, dust grains, electrons from the sun, solar wind, and cosmic rays. Life on Earth relies on the sun for the provision of essential heat energy. Beyond warmth and light, the sun contributes to the creation of the blue sky, clouds, rain, snow, trees, flowers, flowing streams, and the oxygen vital for our existence. Humans have harnessed solar energy throughout history, utilizing it in various forms, from burning wood to fossil fuels like coal, oil, gasoline, and natural gas. Even wind and water energy trace their origin to the sun, as heat generates wind and drives the water cycle, sustaining the world's ecosystems. The sun undergoes constant changes, marked by violent explosions within. These changes extend to its magnetic field. While sunlight is crucial for life, it carries potential dangers in the form of gamma rays, x-rays, ultraviolet rays, and high-energy atomic particles. Earth's protective mechanisms, including ozone, atomic oxygen, nitrogen, and the magnetic field, shield against these harmful radiations, preventing extinction and facilitating life's evolution. Despite these defenses, cosmic rays from the sun and distant particles can penetrate the Earth, with the sun's magnetic cycle influencing their intensity. Earth's magnetic field acts as a shield against cosmic rays, but their concentration increases during periods of solar minimum. Monitoring these cosmic rays is essential for understanding their impact on Earth. The Earth's atmosphere provides partial protection against solar radiation, leading to phenomena like the aurora when radiation interacts with the magnetic field. Harmful rays, such as UV-A and UV-B, can still reach the Earth, posing potential risks depending on atmospheric thickness and variations. Space exploration, initiated in the late 1940s and expanded by NASA in 1958, has revealed crucial insights into the sun's nature, the near-Earth environment, magnetic fields, and atmospheres. Discoveries include the constant flow of solar particles, solar eruptions, and the turbulent conditions near Earth. Solar fluctuations influence Earth's climate and communication systems, affecting everything from telephones to navigation systems. High-altitude aircraft, electrical grids, electronic equipment, and living organisms are also impacted. Our understanding of the Sun-Earth system evolves continuously, leading to interdisciplinary studies such as Heli physics. This comprehensive science explores interconnected systems, utilizing analytical models to simulate solar events' effects on Earth and human activities.

THE SUN, THE EARTH, AND NEAR-EARTH SPACE courses are specifically designed for teachers, students, researchers, and anyone interested in studying the solar system. Effects of the Sun on the Earth space exploration atmosphere around the earth and the magnetic field generated by the sun. The Sun-Earth System: contents as follows:

1. **The Sun**

   This section explores the sun's impact on Earth, encompassing both beneficial and harmful effects. It delves into solar phenomena, such as magnetic fields generated by solar eruptions and solar wind, influencing various celestial bodies, including Earth. Despite the sun's potential harm, Earth's enveloped atmosphere adeptly manages its effects.

2. **The Solar Wind & Solar Variability**

   The solar wind phenomenon results from various atoms and molecules, with electrons forming a magnetic field. The speed of the solar wind varies, spreading in all directions and reaching Earth's orbit in just two days at its highest speed. The section discusses solar events occurring over many years and predicts the solar cycle. It also explores the phenomenon of illumination, the birth of propagated magnetic fibers, and includes data on the sun's energy produced by the solar cycle, along with various other interesting details.

3. **The Near-Earth Environment**

   This section underscores the Earth's atmosphere and environment as remarkably protective against the sun's harmful effects. Whether it is atoms or various molecules, including nitrogen, everything in the air acts as a formidable shield against solar radiation. The text also notes that the temperature changes occurring with altitude are a phenomenon caused by sunlight and the Earth's surrounding atmosphere. Detailed information about the Earth's atmosphere is provided, including an elaborate explanation of Earth's radiation belts.

4. **Fluctuations in Solar Radiation at the Earth**

   This section delves into the dynamic changes in the sun occurring constantly, encompassing eruptions, sunspots, and various events, each with its distinct time frame. It emphasizes that these fluctuations, though uncontrollable, can be compensated for. The Sun's magnetic field undergoes variations from daily to monthly to yearly, resulting in a solar cycle marked by magnetic field changes. The topic also explores the energy received from the sun by the Earth, discussing the phenomenon arising from the Earth's rotation around the sun, its impact on Earth's orbit, and the intriguing occurrence of some sunlight disappearing before reaching Earth.

5. **Variation in the Flow of Particles at the Earth**

   This section explores the fluctuations in different particles originating from sunlight reaching Earth. It details the loss of electrons due to the partial disappearance of sunlight, the motion of the solar wind, and their impact on generating electrical charges. These processes influence changes in the magnetic field, creating a proton current with the potential to penetrate 4 inches of steel. The discussion includes the solar energy source, particles produced by solar flares, the effects of moving solar flare particles, impacts of solar wind plasma, solar wind speed, and magnetic field effects. It also covers the effects of cosmic radiation and other captivating natural phenomena.

6. **Impacts of Solar Variability**

   The interconnectedness of solar events and their impact on Earth, Solar activities, such as Coronal Mass Ejections (CMEs) and solar flares, or gradual factors like the Sun's rotation and magnetic activity variations, influence the Earth's environment. These solar-induced impacts encompass hazards in near-Earth and space environments, disturbances in Earth's magnetosphere, electric currents in the atmosphere, changes in the ionosphere, and increased heating of the lower atmosphere, Earth's surface, and oceans. The effects span a wide range of activities, including satellite communication, news broadcasting, spaceflight, power transfer, national security, financial transactions, weather, climate, and human health.

7. Effects on Human Life and Endeavor

The alteration of Earth's near-space environment by solar disturbances, including changes in the magnetosphere, ionosphere, atmosphere, oceans, and solid surface, has profound impacts on various aspects of human life and activities. Over the past two hundred years, our understanding of these effects has evolved, initially centered on sunspots and auroral displays and later expanding with technological advancements.

Aircraft travel: Solar disturbances can lead to disruptions in operational flight control and aircraft communication. High-altitude polar flights are particularly vulnerable to exposure to solar particles, and there's potential for disruption in ground-to-air and air-to-ground communications.

Human space flight: Astronauts during spaceflights, both inside and outside spacecraft, face increased exposure to high-energy particles. During Extravehicular Activities (EVAs) or while on the Sun-lit surfaces of the Moon or Mars, astronauts are vulnerable to enhanced x-ray emission.

Operation of spacecraft and space equipment: Various factors impact the operation of spacecraft and space equipment. These include electrical charging leading to metallic surface degradation, induced charging affecting computer memory and processors, damage to semiconductor devices, orbital perturbations, accelerated orbital decay, degradation of solar cell surfaces, disruption of spacecraft attitude control, and interference with low-altitude satellite tracking.

Observations of the earth from space: Solar disturbances can result in the interruption and degradation of data crucial for meteorological forecasts, hurricane tracking, crop yield forecasting, and national security surveillance.

Communications and national security: Ionospheric disturbances caused by solar activity can affect radio transmissions and electronic communication across various bands. This impact extends to satellite phones, network television, communications satellites, transmissions to and from orbiting spacecraft, and essential military communications and radar systems.

Geographic position finding and navigation: Solar disturbances can introduce errors and reduce accuracy in GPS systems. Malfunctions of navigational aids and the introduction of magnetic compass errors are also potential effects.

Electric power transmission: Power grids are susceptible to disruptions due to solar-induced currents, leading to power blackouts, brownouts, and failures of power-line transformers.

Operation of oil and gas pipelines: Solar-induced electric currents can lead to corrosion and failure of pipelines, particularly at high latitudes.

Geological surveying and prospecting: Errors and reduced accuracy in geological survey work, including prospecting for minerals and oil, can occur due to solar-driven perturbations and magnetic storm impacts.

Regional and global climate: Solar disturbances impact Earth's surface and subsurface temperatures, influencing atmospheric circulation, precipitation, and broader climate change factors such as El Niños and human-induced greenhouse warming.

8. Effects of the Sun on Weather and Climate

The Sun plays a pivotal role as the primary energy source driving Earth's weather patterns and climatic phenomena. Despite this recognition spanning over two centuries, the extent of the Sun's influence on weather and climate variations remains a topic of ongoing investigation. Historically, dating back to early religions and intuitive notions, there were concerns about the Sun's constancy influencing weather patterns. Even after Galileo's discovery of sunspots in 1609, the link between solar activity and Earth's weather was speculative. The 11-year solar cycle, identified by Heinrich Schwabe in 1843, marked a turning point, but investigations faced challenges until recent advancements provided necessary data. In the late 19th century, claims connecting the sunspot cycle to various phenomena surged, guided by hopes of practical weather prediction. However, statistical correlations with solar activity often fell short. Until the late 20th century, studies relied on statistical comparisons, lacking a robust physical explanation. Solar variability's impact on Earth's weather and climate involves a range of factors:

Meteorological and hydrological effects: Sunspots and solar activity were linked to meteorological and hydrological changes, although rigorous statistical tests were required.

Oceanographic Influences: Solar cycles were associated with oceanographic phenomena, impacting sea surface temperatures and circulation patterns.

Physiological and behavioral connections: Investigations explored potential links between solar activity and human health, behavior, and physiological changes.

Economic factors: Claims in the 19th century included correlations between sunspot cycles and economic indicators, such as wheat prices.

Satellite communication: Solar events can disrupt satellite communication, impacting global communication systems.

Power transfer and electric grids: Solar-induced currents may lead to power blackouts, brownouts, and disruptions in electric power grids.

Aircraft travel: High-altitude polar flights can be exposed to solar particles, potentially disrupting flight control and communication.

Space exploration: Spacecraft and space equipment operation can be affected by electrical charging, degradation of solar cell surfaces, and disruptions in satellite tracking.

Climate change: Solar variability contributes to regional and global climate influences, affecting temperatures, atmospheric circulation, and precipitation.

9. Forecasting Space Weather at the Earth and Beyond

The terms "space weather" and "space climate" describe conditions in Earth's outer environment, akin to "weather" and "climate" referring to the lower atmosphere. Space weather encompasses conditions on the Sun, in the solar wind, near Earth, and in the upper atmosphere, impacting technological systems and human activities. Severe space weather events can lead to economic losses comparable to severe weather phenomena. In today's high-tech world, space weather affects various aspects of life, from television and radio use to air travel and power grids. Unlike terrestrial weather, space weather spans a vast region, from the upper atmosphere to the Sun, impacting ionosphere, thermosphere, magnetosphere, radiation belts, and interplanetary space. Predicting space weather is crucial for minimizing societal impacts. Various users, including airlines, power companies, telecommunications, security agencies, and space exploration entities, rely on predictions. Forecasts, now casts, alerts,

watches, and warnings are types of predictions issued based on computer models replicating the Sun-Earth system's behavior.

After completing the reading of this book, we have not only gained interest but also expanded our theoretical knowledge about the sun, the Earth, and the surrounding space. We are confident that this book holds value due to its well-curated and beneficial information gathered by the author. We utilized this book as a resource for correcting and improving reference data in our research. Furthermore, we believe this book to be a reliable and informative source. We sincerely hope that all readers will greatly benefit from reading this book.

ACKNOWLEDGEMENT

We would like to thank Assistant Professor Dr. Prasert Kenpankho from Space, Satellite, and Study Laboratory (SSS Lab), Department of Engineering Education, King Mongkut's Institute of Technology Ladkrabang, Thailand for consulting on this article.

REFERENCES

Eddy, J. A. (2009). *The sun, the earth, and near-earth space: A guide to the sun-earth system*. National Aeronautics and Space Administration (NASA).

IJIET
INTERNATIONAL JOURNAL
OF INDUSTRIAL EDUCATION AND TECHNOLOGY
ISSN 2673-0448

Research Articles

COMPARISON OF SEVERE GEOMAGNETIC STORM EVENT AND LOW-LATITUDE TOTAL ELECTRON CONTENT ANOMALIES

Wishapol Sittichai[1], Sunadda Koednawee[1], and Chollada Pansong[2*]
E-mail: 66036029@kmitl.ac.th[1], 65036040@kmitl.ac.th[1] and chollada_p@rmutt.ac.th[2*]

Received: December 7, 2023
Revised: December 18, 2023
Accepted: December 25, 2023

ABSTRACT

In this study, we examined the Total Electron Content (TEC) anomalies at different scales during geomagnetic storms using Global Positioning System (GPS) satellites at low latitudes, which contributed to the catastrophic geomagnetic storm that occurred on March 24th, 2023. SIET KMITL, Bangkok station (13.729°N, 100.780°E) and KMITL Chumphon station (10.724°N, 99.375°E), Thailand, are the low-latitude GPS stations. After comparing the two GPS TEC stations, we examined the connection between TEC anomalies in the ionosphere and geomagnetic storm sizes. The findings demonstrate that ionosphere anomalies detected by GPS TEC correlate with geomagnetic storm timing. The findings demonstrate that ionospheric TEC anomalies detected by GPS were noticed that the GPS TEC values at both stations increase in proportion to the strength of the geomagnetic storm on days when the storm's intensity is higher. TEC levels rise progressively during periods of high geomagnetic storm severity. Even after the storm passes, TEC stays raised for two to three days before gradually falling back to normal. The maximum value of TEC, about 35 TECU, was observed at the SIET KMITL, Bangkok station (13.729°N, 100.780°E), whereas TEC increased to about 25 TECU at the KMITL Chumphon station (10.724°N, 99.375°E). TEC is high and positively correlated with an increase in days with intense geomagnetic storms. A rise in the frequency of intense geomagnetic storms is positively connected with TEC. However, in typical circumstances, TECs do not decrease in a negative direction during the quiet period.

Keywords: Geomagnetic storm, GPS TEC, Low-latitude, Total electron content

*Corresponding author E-mail: Chollada_p@rmutt.ac.th
[1]Department of Engineering Education, School of industrial education and technology,
King Mongkut's Institute of Technology Ladkrabang, Bangkok 10520 Thailand
[2*]Department of Technical Education, Faculty of Technical Education, Rajamangala University of Technology Thanyaburi,
Pathum Thani 12110 Thailand

I. INTRODUCTION

A novel avenue for exploring natural dynamics sensing is the use of satellite applications for the Global Positioning Systems (GPS), which provide dependable guidelines. Thus, it is essential to keep enhancing GPS's accuracy and dependability. The quality of GPS satellite transmissions is correlated with the propagation status of the Earth's ionosphere. The ionosphere acts as a middleman to both speed up and slow down signal propagation. The identity of the ionosphere plasma density determines these variations. According to Nayak et al. (2016, pp. 7941-7960), the Total Electron Content (TEC) of the ionosphere influences the phase advance and group delay of GPS satellite signals. The positive ionospheric storms are associated with an enhancement in electron density caused by thermospheric winds, by compositional changes or by the transport of ionization or electric field changes, whereas the negative storms are primarily due to compositional changes of the ionosphere" (Nayak et al., 2016, pp. 7941-7960; Reddybattula et al., 2019, p. 283; Serafimov et al., 1982, pp. 397-399). The main causes of ionospheric anomalies at various latitudes are solar and geophysical-induced perturbations in Earth's space environment. The equatorial and low latitudes around the equator are where changes are most noticeable. An electromagnetic field over the magnetic equator typically has a significant impact on the variation of TEC at low latitudes. Electrical conductivity above the equator significantly increases as a result (Li et al., 2019, p. 9380).

GPS has been used in many researches to display ionospheric abnormalities at different latitudes: high, middle, low, and equatorial. At Chumphon, Thailand, a near equatorial latitude station, Kenpankho et al. (2011, pp. 365-370) conducted a comparison between GPS TEC observations and IRI TEC prediction. Low-latitude TEC variability was investigated by Rao et al. (2013, pp. 1-6) from magnetically conjugate places along 73°E longitude. The 2015 St. Patrick's Day geomagnetic storm prompted studies of the middle-and low-latitude ionosphere reaction by Nava et al. (2016, pp. 3421-3438). By comparing the 28 days running median with the spectral whitening method, Chen et al. (2017, pp. 3632-3639) were able to derive the geomagnetic activity effect from TEC data. During moderate, strong, and extreme geomagnetic storms over the Indian subcontinent, analysis of ionospheric TEC using GPS, Global Ionosphere Map (GIM), and global ionosphere models was conducted (Reddybattula et al., 2019, pp. 283-292). The ionospheric irregularity behavior during the magnetic storm that occurred over the Brazilian equatorial-low latitudes on September 6^{th}-10^{th}, 2017, was examined by de Paula et al. (2019, pp. 1-15). Dugassa et al. (2019, pp. 1161-1180) looked at the connection between the presence of ionospheric abnormalities and the spatial gradient of TEC between two neighboring stations. In the high-latitude ionosphere, Chernyshov et al. (2020, pp. 1-13) reported on the connection between TEC jumps and aurora sub-storms. Ratovsky et al. (2022, pp. 1-15) looked into the relationship between meteorological and geomagnetic activity and extreme ionospheric phenomena. The morphology and processes of the foF2 and TEC disturbances during the geomagnetic storms on September 26^{th}-30^{th}, 2011, were compared and contrasted by Klimenko et al. (2017, pp. 923-938). A global and regional ionospheric response during two geomagnetic storms on February 3^{rd}-4^{th}, 2022, was compared and evaluated by Bojilova and Mukhtarov (2023, pp. 1-23).

In a related study, the response of the middle- and low-latitude ionosphere to the 2015 St. Patrick's Day geomagnetic storm was examined by Nava et al. (2016, pp. 3421-3438). They contrasted the low-latitude station, cusv (Northern Hemisphere), with two middle-latitude stations, Northern Hemisphere (wuhn) and Southern Hemisphere (yar2), for the Asian area. They found a significant decline in the TEC near the middle latitude many days following the storm. At the low latitude, they did discover a rise in TEC on the day of the storm and no decline in the days that followed. Chen et al. (2017, pp. 3632–3639) compared the 28-days running median with the spectrum whitening approach to examine the geomagnetic activity effect from TEC data. They discovered that both the Running Median Centered (RMC) and the Spectral Whitening Method (SWM) assess the ionospheric variations in both quiet and disturbed conditions. When comparing the RMC results to the SWM results, the RMC results overestimate the occurrence of disturbances by approximately 5-20% during geomagnetic storms and up to 35% during quiet periods.

We came up with the idea to gather and compare GPS TEC data from the GNSS receiver and compare the low-latitude TEC disturbances focused on over Bangkok and Chumphon, Thailand, during severe geomagnetic storms on March 24th, 2023. The purpose of the study is to compare TEC anomalies during severe geomagnetic storm event utilizing low-latitude GPS satellites.

II. METHODOLGY

A. Geomagnetic storm data

The Kp index is a physical classification of geomagnetic storm event data. The Space Weather Prediction Center (SWPC), National Oceanic and Atmospheric Administration (NOAA) uses the Kp index to classify geomagnetic storms into five severity levels: G0 (None), G1 (Minor), G2 (Moderate), G3 (Strong), G4 (Severe), and G5 (Extreme). On March 24th, 2023, a severe (G4) geomagnetic storm was observed. Geomagnetic storm data was collected for nine days within the storm period from March 21st to March 29th, 2023, three days before peak of the storm and five days after. The Pushkov Institute of Terrestrial Magnetism, Ionosphere and Radio wave Propagation of the Russian Academy of Sciences (IZMIRAN) website, located at https://www.izmiran.ru /ionosphere/weather/storm/, was where we obtained the hourly geomagnetic storm data for March, 2023. Subsequently, the geomagnetic storm level average every three hours was examined (Kp index), and the data analysis was plotted during the following session.

B. GPS TEC data

In this investigation, low-latitude monitor stations for the Global Navigation Satellite System (GNSS) were located in Bangkok, at SIET KMITL (School of Industrial Education and Technology, King Mongkut's Institute of Technology Ladkrabang), station (13.729°N, 100.780°E) and KMITL Chumphon station (10.724°N, 99.375°E), Thailand. Following the significant geomagnetic storming that was recorded on March 24th, 2023, we collected GPS TEC data in addition to the geomagnetic storm events that occurred three days before and five days after the geomagnetic storm. The GPS TEC was ascertained using the Receiver Independent Exchange Format (RINEX) data obtained from the multi GNSS receiver. The multi GNSS receiver (BG2s GNSS ionospheric monitor model) was used in this work as the data collection tool for GPS TEC. The Institute of Geology and Geophysics, Chinese Academy of Sciences (IGGCAS), provides support for the BG2s GNSS ionospheric monitor system. Figure 1 depicts the connection of the GNSS ionospheric monitor system.

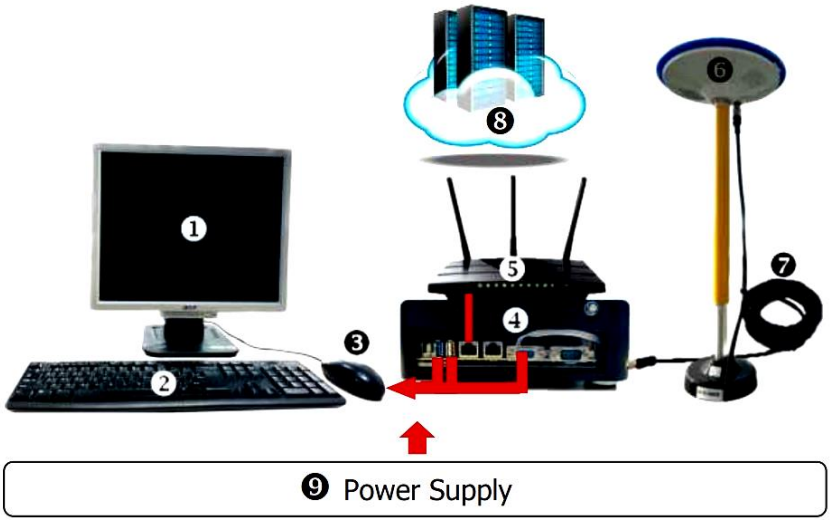

Figure 1 System of BG2s GNSS ionospheric monitor

The GPS system uses two frequencies for signal transmission: f_1 = 1575.42 MHz and f_2 = 1227.60 MHz. Four to twelve GPS signals are continuously received by the GPS receiver. For the GPS TEC computation, RINEX data from the GNSS receiver is utilized. The RINEX file contains pseudo-range (P_1 and P_2) and phase measurements (L_1 and L_2). The difference between the pseudo-ranges (P_1 and P_2) and the phases (L_1 and L_2) of the two frequencies GPS receiver can be used to determine the Slant Total Electron Content (STEC) ($STEC_P$ and $STEC_L$) from a satellite to a receiver (Blewitt, 1990, pp. 199-202; Kenpankho et al., 2011, p. 366). This is the method for calculating values are calculated. The GPS TEC equations, denoted as (1) and (2), are $STEC_P$ and $STEC_L$.

$$\mathrm{STEC_P} = \frac{2\left(f_1 f_2\right)^2}{k\left(f_1^2 - f_2^2\right)}\left(P_2 - P_1\right), \tag{1}$$

$$\mathrm{STEC_L} = \frac{2\left(f_1 f_2\right)^2}{k\left(f_1^2 - f_2^2\right)}\left(L_1\lambda_1 - L_2\lambda_2\right), \tag{2}$$

where the wavelengths corresponding to f_1 and f_2 are represented by λ_1, and λ_2 (λ_1 = 0.1904 m, λ_2 = 0.2444 m), respectively, and k, which is related to the ionosphere refraction, is 80.62 m^3/s^2.

In order to get the GPS TEC, we utilized Equation (2) and entered the parameters (f_1, f_2, L_1, L_2, λ_1, and λ_2) into the equation. Next, we computed Vertical Total Electron Content (VTEC) using Equation (3) and (4). The total electron in a vertical column with a cross-section of one meter is known as GPS TEC (Goodwin et al., 1995, pp. 1723-1732). TEC is measured in TECU unit. One TECU is equal to 10^{16} el/m^2. Equation (3) displays the VTEC, expressed in el/m^2, which may be calculated using the STEC (Kenpankho et al., 2011, p. 366; Ma & Maruyama, 2003, p. 2084).

$$\mathrm{VTEC} = \mathrm{STEC}_L \times \cos\chi, \tag{3}$$

where the zenith angle χ is expressed as

$$\chi = \arcsin\left(\frac{R_E \cos\alpha}{R_E + h}\right), \tag{4}$$

where R_E is the mean radius of the Earth ≈ 6,371 km, α is the satellite's elevation angle, h as the height of the ionospheric layer, which is estimated to be 400 km (Kenpankho et al., 2011, p. 366; Ma & Maruyama, 2003, p. 2084).

Finally, we used GPS TEC data following geomagnetic storm events according to hourly Kp index levels using median statistic.

C. Correlation coefficient

The correlation coefficient can be analyzed from Equation (5) (Mukaka, 2012, p. 69) following as

$$r = \frac{\sum_{i=1}^{n}(x_i - x)(y_i - y)}{\sqrt{\left[\sum_{i=1}^{n}(x_i - \bar{x})^2\right]\left[\sum_{i=1}^{n}(y_i - \bar{y})^2\right]}} \tag{5}$$

where, r is the correlation coefficient of the linear relationship between the variables x and y, x_i is the value of the scale of geomagnetic storm in a sample, $\bar{x}$ is the average of the scale of geomagnetic storm value, y_i is the values of the TEC in a sample, and $\bar{y}$ is the median of the TEC value. The correlation coefficient meaning is in Table 1 as follows.

Table 1 Size interpretation of a correlation coefficient.

Size of correlation	Interpretation
0.90 to 1.00 (−0.90 to −1.00)	Very high positive (negative) correlation
0.70 to 0.90 (−0.70 to −0.90)	High positive (negative) correlation
0.50 to 0.70 (−0.50 to −0.70)	Moderate positive (negative) correlation
0.30 to 0.50 (−0.30 to −0.50)	Low positive (negative) correlation
0.00 to 0.30 (0.00 to −0.30)	Negligible correlation

The datasets were used to calculate the correlation between geomagnetic storm levels and TEC anomalies in low-latitude regions. In this study, we utilized the Kp index levels as an indicator of geomagnetic storm intensity from March 21st to 29th. The GPS TEC values for hourly intervals from the SIET KMITL station (13.729°N, 100.780°E) and KMITL Chumphon station (10.724°N, 99.375°E) were computed to determine the correlation corresponding to each geomagnetic storm day with the Kp index levels. The datasets covered the period from 00:00 to 24:00 UT for each day, spanning March 21st to 29th, 2023.

III. RESULTS

A. Geomagnetic storm levels

Geomagnetic storm level data were acquired for the March 21st, 2023, to March 29th, 2023, timeframe. Figure 2 displays the average hourly geomagnetic storm.

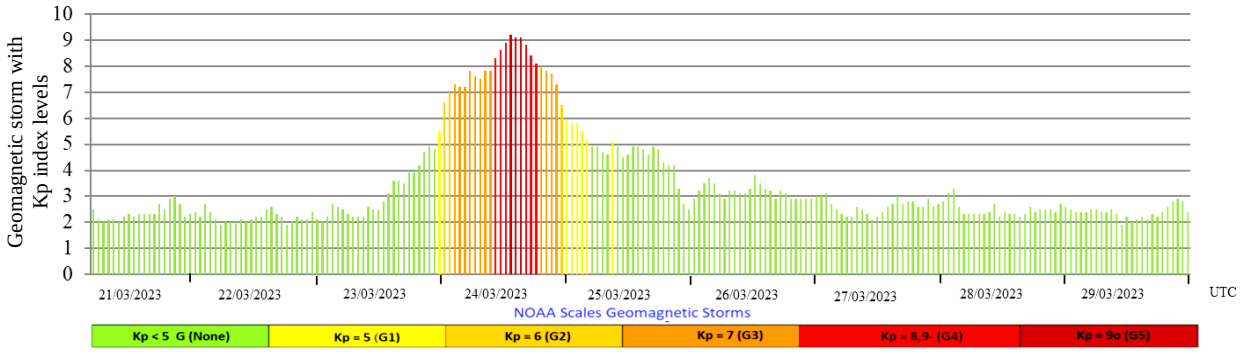

Figure 2 Geomagnetic storm levels that occurred during March 21st, 2023 to March 29th, 2023.

The geomagnetic storm data in Figure 2, which was gathered between March 21st and March 29th, 2023, indicated that there were geomagnetic storm watches in place from March 23rd to March 25th. As the storm continued throughout the late hours of March 23rd, it became stronger into G1, G2, and G3. Furthermore, a G3 episode was observed in the afternoon on March 23rd and strengthened to extreme storm (G5) levels at 12:04 UTC on the 24th. On March 24th, the geomagnetic storms had an average strength that was at the severe storm (G4) category. Following that, on March 25th, the storm's intensity dropped, and the following day, it was back to normal.

B. TEC anomalies compare with geomagnetic storm levels

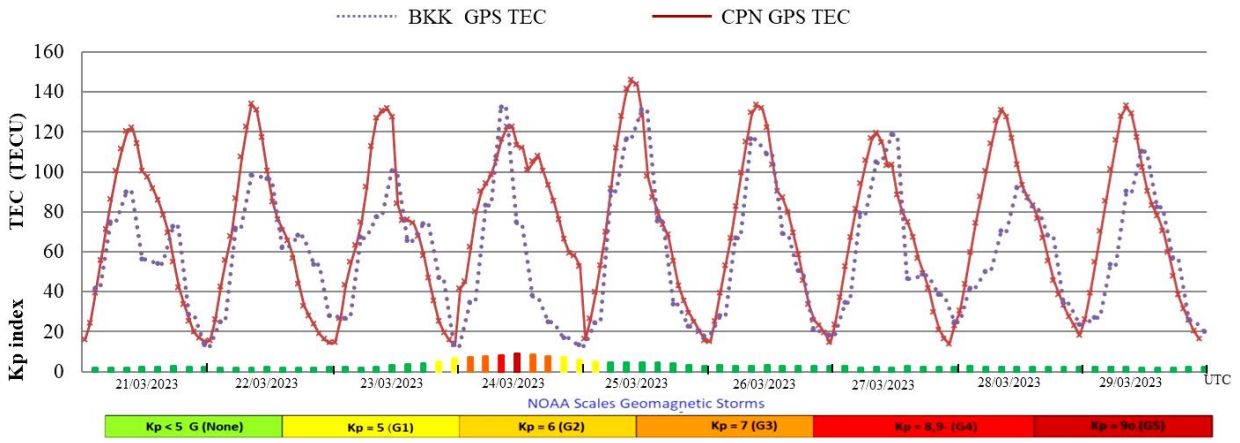

Figure 3 GPS TEC anomalies compare with geomagnetic storm levels at SIET KMITL station (13.729°N, 100.780°E) and KMITL Chumphon station (10.724°N, 99.375°E).

In Figure 3, it can be observed that on days with higher levels of geomagnetic storms, both CPS TEC values at the two stations increase in accordance with the intensity of the geomagnetic storm. The TEC values gradually rise during periods of increased geomagnetic storm intensity, and even when the storm subsides, TEC remains elevated for approximately 2-3 days before gradually decreasing to normal conditions. It was found that at the SIET KMITL, Bangkok station (13.729°N, 100.780°E), TEC reached its highest value, approximately 35 TECU, while at the KMITL Chumphon station (10.724°N, 99.375°E), TEC increased to around 25 TECU. It is clear that the KMITL Chumphon station has greater TEC values than the SIET KMITL, Bangkok station when comparing the TEC values at low-latitude zones between the two stations.

C. The relationship between TEC anomalies and geomagnetic storm levels

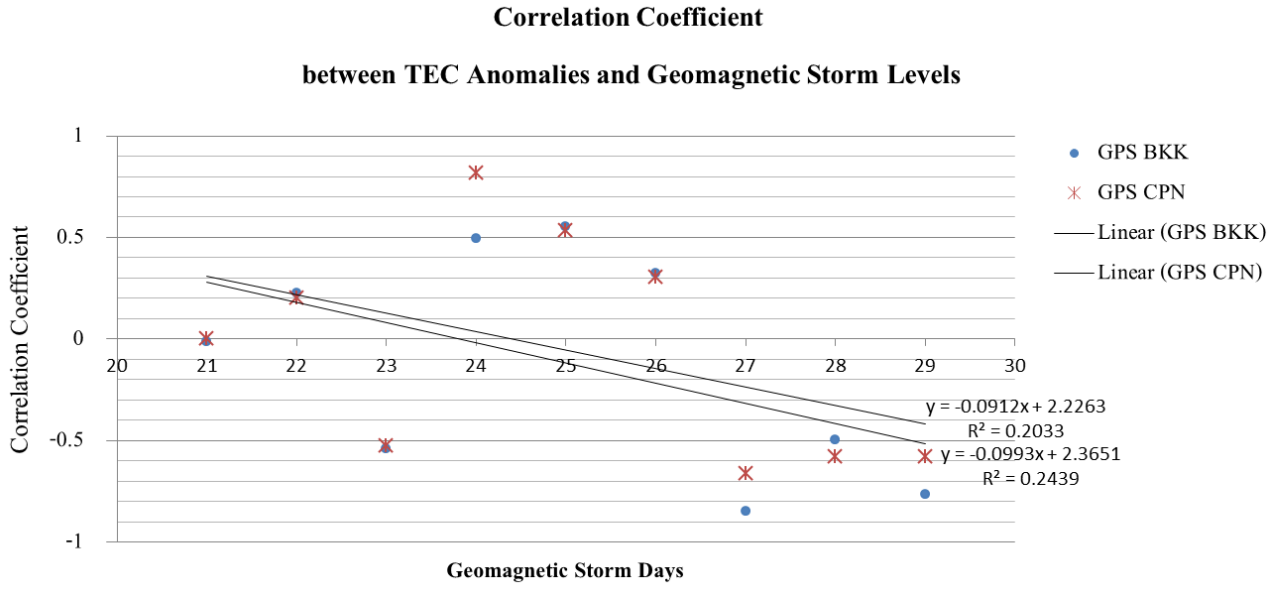

Figure 4 Correlation between TEC anomalies is significantly related to the level of geomagnetic storms.

Figure 4 shows that there is a considerable association between the level of geomagnetic storms and TEC abnormalities. For an increase in strong geomagnetic storms days, TEC is high in a positive direction correlation. TEC is highly correlated in a positive direction with a rise strong geomagnetic storms days. However, during the quiet period, TECs do not drop under normal conditions in a negative direction correlation.

IV. CONCLUSION AND DISCUSSION

In conclusion, we observed the behavior of the TEC at different scales during geomagnetic storms using low-latitude GPS satellites. Ionosphere anomalies detected by GPS TEC two stations at SIET KMITL, Bangkok station (13.729°N, 100.780°E), and KMITL Chumphon station (10.724°N, 99.375°E) correlate with geomagnetic storm-time. A few days after a geomagnetic storm, TECs tend to constantly increase before declining to normal. The degree of geomagnetic storm activity is strongly correlated with TEC abnormalities. When there is a rise in powerful geomagnetic storms, there is a high positive association between TECs. However, under typical circumstances, TECs do not decrease during the quiet period.

In discussion, our research backs up the findings of Chen, et al. (2017, pp. 3632-3639), who examined the geomagnetic activity effect from TEC data and compared the 28-days running median with the spectrum whitening approach. Ionospheric changes in quiet and disturbed settings exaggerate the occurrence of disturbances in tranquil periods and during geomagnetic storms. This study shows that the geomagnetic storm and TEC behavior are similar at low latitudes to those where middle- and low-latitude ionosphere reaction to geomagnetic storm was investigated by Nava et al. (2016, pp. 3421-3438). The study demonstrates a strong association between the storm's aftermath at the middle latitude and a notable decline in the TEC over a few days. At low latitudes, there is an increase in TEC on the day of the storm and no drop in the days that follow. The TEC is confined to low latitudes close to the equator in the days following the storm, and it nearly vanishes in middle latitudes.

ACKNOWLEDGEMENT

We would like to thank the Institute of Geology and Geophysics, Chinese Academy of Sciences (IGGCAS) and Earthquake Observation Division (EOD), Thai Meteorological Department (TMD) for supporting BG2s GNSS receiver and sharing data. We would like to thank Space Weather Prediction Center (SWPC), National Oceanic and Atmosphere Administration (NOAA) organization for sharing data of the geomagnetic storm activity and The Pushkov Institute of Terrestrial Magnetism, Ionosphere and Radio wave Propagation of the Russian Academy of Sciences (IZMIRAN), for hourly geomagnetic storm with Kp index data sharing. We would like to thank Assistant Professor Dr. Prasert Kenpankho from Study, Satellite, and Space Laboratory, Department of Engineering Education, King Mongkut’s Institute of Technology Ladkrabang, Thailand for consulting this research.

REFERENCES

Blewitt, G. (1990). An automatic editing algorithm for GPS data. *Geophysical Research Letters, 17*(3), 199-202.

Bojilova, R., & Mukhtarov, P. (2023). Comparative analysis of global and regional ionospheric responses during two geomagnetic storms on 3 and 4 February 2022. *Remote Sensing, 15*(7), 1-23.

Chen, Z., Wang, J. S., Deng, Y., & Huang, C. M. (2017). Extraction of the geomagnetic activity effect from TEC data: A comparison between the spectral whitening method and 28 day running median. *Journal of Geophysical Research: Space Physics, 122*(3), 3632-3639.

Chernyshov, A. A., Miloch, W. J., Jin, Y., & Zakharov, V. I. (2020). Relationship between TEC jumps and auroral substorm in the high-latitude ionosphere. *Scientific Reports, 10*(6363), 1-13.

Nayak, C., Tsai, L. C., Su, S. Y., Galkin, I. A., Tan, A. T. K., Nofri, E., & Jamjareegulgarn, P. (2016). Peculiar features of the low-latitude and midlatitude ionospheric response to the St. Patrick's Day geomagnetic storm of 17 March 2015. *Journal of Geophysical Research: Space Physics, 121*(8), 7941-7960.

de Paula, E. R., de Oliveira, C. B. A., Caton, R. G., Negreti, P. M., Batista, I. S., Martinon, A. R. F., Neto, A. C., Abdu, M. A., Monico, J. F. G., Sousasantos, J., & Moraes, A. O. (2019). Ionospheric irregularity behavior during the September 6-10, 2017 magnetic storm over Brazilian equatorial–low latitudes. *Earth, Planets and Space, 71*(42), 1-15.

Dugassa, T., Habarulema, J. B., & Nigussie, M. (2019). Investigation of the relationship between the spatial gradient of total electron content (TEC) between two nearby stations and the occurrence of ionospheric irregularities. *Annales Geophysicae*, *37*(6), 1161-1180.

Goodwin, G. L., Silby, J. H., Lynn, K. J. W., Breed, A. M., & Essex, E. A. (1995). GPS satellite measurements: ionospheric slab thickness and total electron content. *Journal of Atmospheric and Terrestrial Physics, 57*(14), 1723-1732.

Kenpankho, P., Watthanasangmechai, K., Supnithi, P., Tsugawa, T., & Maruyama, T. (2011). Comparison of GPS TEC measurements with IRI TEC prediction at the equatorial latitude station, Chumphon, Thailand. *Earth, Planets and Space, 63*, 365-370.

Klimenko, M. V., Klimenko, V. V., Zakharenkova, I. E., Ratovsky, K. G., Korenkova, N. A., Yasyukevich, Y. V., Mylnikova, A. A., & Cherniak, I. V. (2017). Similarity and differences in morphology and mechanisms of the foF2 and TEC disturbances during the geomagnetic storms on 26-30 September 2011. *Annales Geophysicae*, *35*(4), 923-938.

Li, G., Ning, B., Zhao, X., Sun, W., Hu, L., Xie, H., Liu, K., & Ajith, K. K. (2019). Low latitude ionospheric TEC oscillations associated with periodic changes in IMF Bz polarity. *Geophysical Research Letters, 46*(16), 9379-9387.

Ma, G., & Maruyama, T. (2003). Derivation of TEC and estimation of instrumental biases from GEONET in Japan. *Annales Geophysicae*, *21*(10), 2083-2093.

Mukaka, M. M. (2012). Statistics corner: A guide to appropriate use of correlation coefficient in medical research. *Malawi Medical Journal*, *24*(3), 69-71.

Nava, B., Rodríguez-Zuluaga, J., Alazo-Cuartas, K., Kashcheyev, A., Migoya-Orué, Y., Radicella, S. M., Amory-Mazaudier, C., & Fleury, R. (2016). Middle- and low-latitude ionosphere response to 2015 St. Patrick's Day geomagnetic storm. *Journal of Geophysical Research: Space Physics, 121*, 3421-3438.

Rao, S. S., Galav, P., Sharma, S., & Pandey, R. (2013). Low-latitude TEC variability studied from magnetically conjugate locations along 73° E longitude. *Journal of Atmospheric and Solar-Terrestrial Physics, 104*, 1-6.

Ratovsky, K. G., Klimenko, M. V., Dmitriev, A. V., & Medvedeva, I. V. (2022). Relation of extreme ionospheric events with geomagnetic and meteorological activity. *Atmosphere, 13*, 1-15.

Reddybattula, K. D., Panda, S. K., Ansari, K., & Peddi, V. S. R. (2019). Analysis of ionospheric TEC from GPS, GIM and global ionosphere models during moderate, strong, and extreme geomagnetic storms over Indian region. *Acta Astronautica, 161*, 283-292.

Serafimov, K. B., Arshinkov, I. S., Bochev, A. Z., Petrunova, M. H., Stanev, G. A., & Chapkanov, S. K. (1982). A measuring equipment for electric and magnetic fields in the range of the ionosphere-Magnetosphere plasma mounted aboard the "Intercosmos-Bulgaria 1300" satellite. *Acta Astronautica, 9*(6-7), 397-399.

SKY PLOT VISIBILITY BASED ON BEIDOU AND GPS SATELLITES OVER BANGKOK, THAILAND

Thanapon Keokhumcheng[1*], Bussara Pasew[2], and Tawatchai Samosol[2]
E-mail: kpongthanaponok@gmail.com[1*], 65036091@kmitl.ac.th[2], and 65036087@kmitl.ac.th[2]

Received: December 12, 2023
Revised: December 24, 2023
Accepted: December 28, 2023

ABSTRACT

The Global Navigation Satellite System (GNSS) over the Bangkok region occasionally has spots where its performance could be more consistent and imprecise due to the dust in the sky, the surroundings, and high buildings. As a reason, the area has an impact on satellite signal reception. As a reason, the area has an impact on satellite signal reception. As a reason, the area has an impact on satellite signal reception. It blocks and reflects satellite signals and more than the visibility of GNSS satellites is needed to be useful. We offer a sky visibility analysis based on satellites classification. We provide information on sky visibility estimation for BeiDou and GPS satellites based on direct GNSS receiver measurements. The visibility of BeiDou and GPS satellites is classified by sky plotting techniques. For our proposed analytical evaluation of the visibility satellites over Bangkok on November 8th, 2023, we found that the locations of BeiDou and GPS satellites were at different times and affected the efficiency of analyzing the visibility of sky plots throughout Bangkok, Thailand.

Keywords: Sky visibility, BeiDou satellite, GPS satellite, Sky plot, GNSS

*Corresponding author E-mail: kpongthanaponok@gmail.com
[1*]Department of Electronic, Nongbualumphu Technical Collage, Nongbualumphu 39000 Thailand
[2]Department of Engineering Education, School of Industrial Education and Technology,
King Mongkut's Institute of Technology Ladkrabang, Bangkok 10520 Thailand

I. INTRODUCTION

The positioning systems based on the GNSS are now considered an important technology for daily life. Especially this technology is used to determine position such as car navigation systems, transportation systems, and aviation systems. Relying on this system must avoid buildings that may obscure the satellite signal. For example, large urban areas like Bangkok have used this technology because there are surrounding buildings that block or affect the reception of satellite signals. Positioning system services based on GNSS are used daily. GNSS positioning is an important technology such as car navigation and real-time monitoring of Sanitation vehicles in cities. However, GNSS positioning performance in a big city could be more satisfactory due to the surrounding buildings blocking or interfering with some satellite signals. Therefore, this affects the positioning error in these areas for upper a hundred meters (An et al., 2020, pp. 1-13; Dabove & Pietra, 2019, pp. 1-17; Garcez et al., 2019, pp. 1-15; Geng et al., 2019, pp. 977-991; Hamza et al., 2023, pp. 1-19). GNSS positioning is a popular approach for improving this urban GNSS positioning performance in which GNSS system analysis like GPS, BeiDou Galileo, GLONASS, IRNSS, and QZSS satellites are used to analyze and predict the satellites sky plot visibility over Bangkok, Thailand.

For GNSS testing, (Hamza et al., 2020 & 2021, pp. 1-16; Huang et al., 2021, pp. 1-20; Yang & Shim (2013, pp. 199-204), they investigated the GNSS signals and simulated the transmitting path, Carrier-to-Noise ratio (C/No) of satellite signals, planimetric plot, and cumulative loss of continuity. Jia et al. (2022, pp. 1-9) experimented by using a single frequency GNSS receiver for analyzing the GNSS satellites signals. They used the single-epoch attitude for determining method with orthogonal constraints for GNSS. BeiDou and GPS satellites can be divided into different positions based on their presence on the sky visibility are applying by Li et al. (2014, pp. 72-89) presented real-time GNSS seismology using a single receiver. Xu et al. (2020, pp. 1-15) presented method sky visibility estimation based on GNSS satellite visibility: an approach of GNSS-based context awareness and Zhang et al. (2020, pp. 1-21) who used a single-receiver geometry-free approach to stochastic modeling of multi-frequency GNSS observables. We offer an analysis that can provide information on sky visibility predictions for BeiDou and GPS satellites based directly on GNSS receiver measurements. Colagrossi et al. (2020, pp. 1-30) describe the methodologies and the proposed strategies to overcome the mission limitations, while achieving a satisfactory constellation visibility of the sky throughout the mission duration. Cai et al. (2015, pp. 133-143) investigating the quad-constellation precise point positioning (PPP) for position determination and analyzing its positioning performance. A quad-constellation PPP model is developed to simultaneously process the observations from GPS, BeiDou, GLONASS and Galileo satellites systems. Lu and Han (2020, pp. 123-128) proposes using superimposed column method to analyze GNSS receivers'surrounding environments and thus improve GNSS satellite visibility predictions in an efficient and reliable manner. Kenpankho et al. (2021, pp. 2152-2159) applied a multi-frequency GNSS receiver to find real-time GPS receiver bias estimation. Liu et al. (2021, pp. 1-12) found the characteristics of phase bias and GNSS application in multi-frequency and multi-GNSS PPP with ambiguity resolution. Wielgocka et al. (2021, pp. 1-14) found the feasibility of using low-cost dual-frequency GNSS receivers for land surveying. In addition, Mao et al. (2021, pp. 1-13) solved the problem on the delay time from GNSS satellites signals according to a new simplified zenith tropospheric delay model for real-time GNSS applications. For the GNSS performance investigation, Odolinski and Teunissen (2020, pp. 1-17) found the best integer equivariant estimation: performance analysis using real data collected by low-cost, single-and dual-frequency, multi-GNSS receivers for short- to long-baseline real-time kinematic positioning (RTK) positioning. Tu et al. (2021, pp. 345-355) investigated the precision of frequency transfer model suitable for short baseline link based on GPS single-differenced observations with ambiguity

resolution. Moreover, Ding et al. (2023, pp. 1-13) investigated the performance analysis of a normal GNSS receiver model under different types of jamming signals.

After studied the research, there was found that one research project used to verify GNSS, which is the examination of BeiDou and GPS satellites over Bangkok Thailand. It was interested in studying the appearance of satellites between BeiDou and GPS over Bangkok Thailand on November 8th, 2023, a day during which there was a severe change in the Earth's magnetic field, in where researchers can determine the GNSS receiver is located, allowing BeiDou and GPS satellite in that GNSS system can be applied. BeiDou and GPS satellites can be divided into different positions based on their presence on the sky visibility are applying by Li et al. (2014, pp. 72-89) who presented the real-time GNSS seismology using a single receiver and Zhang et al. (2020, pp. 1-21) used a single-receiver geometry-free approach to stochastic modeling of multi-frequency GNSS observables. We offer an analysis that can provide information on sky visibility predictions for BeiDou and GPS satellites based directly on GNSS receiver measurements.

The statement of research purpose is inspired using a multi-GNSS receiver application. The visibility of BeiDou and GPS satellites can be classified by sky plot technique. For assessing the sensitivity of our proposed sky plot visibility analysis, we used a multi-GNSS receiver for receiving BeiDou and GPS satellites signals that are in different time periods and effects on the performance on the analysis of sky plot visibility over Bangkok, Thailand.

II. METHODOLOGY

A. Research procedure

According to the research studies and related research information, we studied the visibility of GPS satellites and BeiDou satellites over Bangkok, Thailand. The research processes were procedures step by step: First, the collected observer BeiDou and GPS satellite signal data and classified it by include periods of time are sunrise, noon, sunset, and midnight. Then, we collected BeiDou and GPS satellites positioned signal data using multi frequency.

B. Data collection

In the studies, we collected BeiDou and GPS satellites data from a multi GNSS receiver at SIET KMITL station Bangkok, Thailand, (13.729°N, 100.780°E). We collected BeiDou and GPS satellites data following observed on November 8th, 2023, there are changes Total Electron Content (TEC) in the ionosphere to magnetic field changes in the earth. Satellites data were collected into four time according to the phase of sun periods: sunrise (6:00 o'clock), noon (12:00 o'clock), sunset (18:00 o'clock), and midnight (00:00 o'clock). In this study, the multi GNSS receiver (BG2s GNSS ionospheric monitor model) was the instrument to collect BeiDou and GPS satellites signals data. The BG2s GNSS ionospheric monitor system is supported by Geology and Geophysics, Chinese Academy of Sciences (IGGCAS). The GNSS ionospheric monitor system connection is shown in Figure 1 as the BG2s GNSS ionospheric monitor.

Figure 1 BG2s GNSS ionospheric monitor system.

C. Data analysis

The visibility of the global navigation satellite system is positioning above the sky at the location where the GNSS receiver is installed locating, distinguishing numbers, and signal information of the global navigation satellite system, that can be observations from satellite receivers at that time. All information displayed can only be viewed by using GNSS receiver and assume of the information which are positioning displayed of each satellite above that location. The different heights, strength of the satellite signal transmitted. GPS satellites and BeiDou satellites received from GNSS receivers are using to display the visibility of the global navigation satellite system in the regions around the world. The visibility of the BeiDou and GPS satellites can be created using a simulated sky based on the Earth's elevation line of 0° from the ground up to a perpendicular point of 90° above the area where the global navigation satellite receiver is installed and divided the angles of the directions that angle 0° is north, 90° is east, 180° is south, angle 270° is west, and finally at 360° is north again. The sky plot visibility mask generated from GNSS receiver, BG2s ionospheric monitor, is calculated by the elevation angle and azimuth angle can be expressed as in Equation (1). There are $elev_{Az}$ for the elevation angle of a particular azimuth angle Az, which ranges from 1° to 360°, $elev_R$ for elevation angle 90°, and Az_D for azimuth angle direction of GNSS receiver, BG2s ionospheric monitor, position 360° (Xu et al., 2020, pp. 1-15).

$$\text{Sky plot visibility} = \frac{\sum_{Az=0^\circ}^{360^\circ} elev_{Az}}{elev_R \times Az_D} \quad (1)$$

where $elev_R$ is 90°, and Az_D is 360°

III. RESULTS

This study research collected BeiDou and GPS satellites data as the results, from a multi GNSS receiver at SIET KMITL station over Bangkok, Thailand. We collected BeiDou and GPS satellites data following observed for a day on November 8th, 2023. Satellites data were collected into four time periods at 06:00 o'clock for sunrise, 12:00 o'clock for noon, 18:00 o'clock for sunset, and 00:00 o'clock for midnight according to the phase of sun. According to the Equation 1, the sky plot visibilities of BeiDou and GPS satellites were plotted into four times including for sunrise, noon, sunset, and midnight as shown in Figure 2 which BeiDou and GPS sky plot visibilityes on November 8th, 2023, are shown respectively.

In Figure 2, the result of observed number of satellites were BeiDou and GPS sky plot visibilities over Bangkok, Thailand on November 8th, 2023. There is a comparison of the number of satellites which are displayed by the BG2s satellite receiver in each period which is divided into four time periods: 6:00 a.m., sunrise time, 12:00 p.m., noon time, 6:00 p.m., sunset time, and finally 12:00 a.m., midnight time.

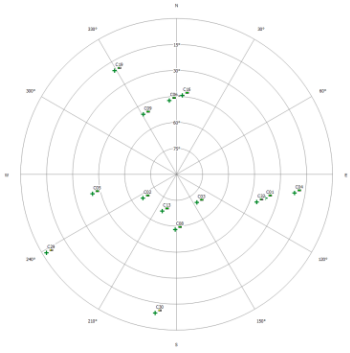

a) BeiDou sky plot visibilities at 06:00 am.

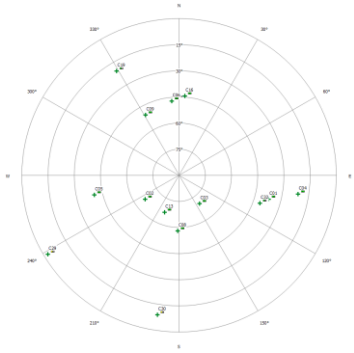

b) GPS sky plot visibilities at 06:00 am.

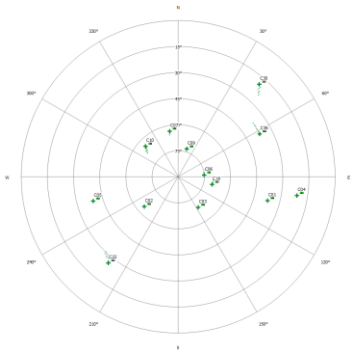

c) BeiDou sky plot visibilities at 12:00 am.

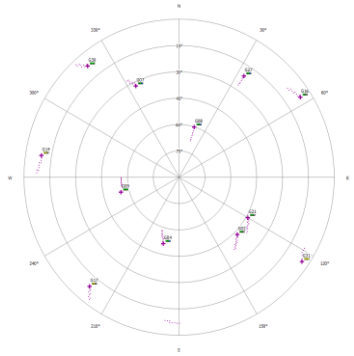

d) GPS sky plot visibilities at 12:00 am.

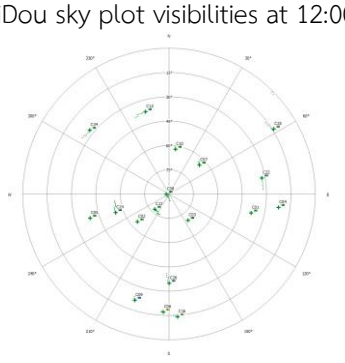

e) BeiDou sky plot visibilities at 18:00 pm.

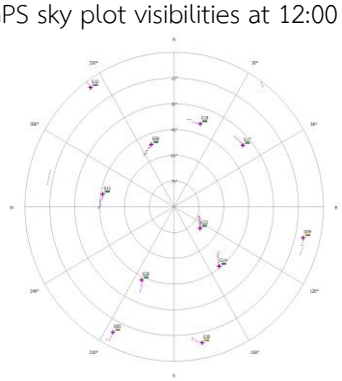

f) GPS sky plot visibilities at 18:00 pm.

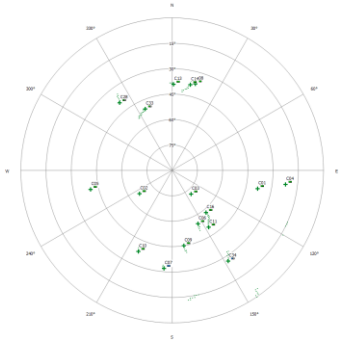

g) BeiDou sky plot visibilities at 00:00 am.

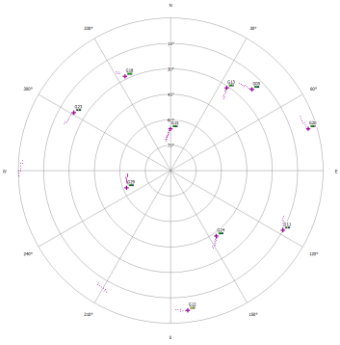

h) GPS sky plot visibilities at 00:00 am.

Figure 2 BeiDou and GPS sky plot visibilities on November 8th, 2023.

The BeiDou satellites visibilities at local time (LT) over Bangkok On November 8th, 2023, show in Table 1. There are 38 BeiDou satellites in the satellite number preceded by a letter indicating "C". There are 38 BeiDou satellites that are visibility on sky plot excluding C15, C17, C18, C20, C21, C23, C27, C31, C33, C34, C35, C37, and C38. There are C1, C2, C3, C4, C5, C6, C9, C10, and C16 that can be received for four periods of time. The BeiDou satellites that can be received all three periods of time are C7, C8, and C13. There are satellites that can received two periods of time which are C8, C19, C22, C24, and C30. Other than that can be received one periods of time as show in Table 1.

Table 1 BeiDou satellites visibilities over Bangkok on November 8th, 2023.

No.	Time (LT)	06:00		12:00		18:00		00:00	
	Satellite	Azimuth	Elevation	Azimuth	Elevation	Azimuth	Elevation	Azimuth	Elevation
1	C1	105°	37°	105°	37°	103°	38°	102°	38°
2	C2	235°	66°	229°	64°	229°	64°	235°	66°
3	C3	144°	70°	147°	69°	144°	70°	141°	72°
4	C4	99°	21°	99°	21°	97°	22°	97°	22°
5	C5	257°	40°	254°	39°	253°	39°	257°	40°
6	C6	352°	47°	73°	73°	184°	18°	154°	51°
7	C7	-	-	348°	63°	46°	64°	185°	32°
8	C8	178°	58°	-	-	266°	89°	12°	36°
9	C9	328°	59°	16°	70°	199°	23°	170°	41°
10	C10	173°	32°	308°	64°	8°	62°	203°	38°
11	C11	-	-	-	-	-	-	141°	50°
12	C12	-	-	-	-	344°	38°	144°	0°
13	C13	200°	67°	-	-	223°	77°	0°	38°
14	C14	-	-	-	-	-	-	7°	38°
15	C15	-	-	-	-	-	-	-	-
16	C16	2°	44°	92°	69°	178°	15°	141°	54°
17	C17	-	-	-	-	-	-	-	-
18	C18	-	-	-	-	-	-	-	-
19	C19	326°	15°	-	-	46°	1°	-	-
20	C20	-	-	-	-	-	-	-	-
21	C21	-	-	-	-	-	-	-	-
22	C22	-	-	219°	26°	87°	32°	-	-
23	C23	-	-	-	-	-	-	-	-
24	C24	-	-	-	-	263°	56°	114°	14°
25	C25	-	-	-	-	-	-	168°	13°

Table 1 (continued) BeiDou satellites visibilities over Bangkok on November 8th, 2023.

No.	Time (LT)	06:00		12:00		18:00		00:00	
	Satellite	Azimuth	Elevation	Azimuth	Elevation	Azimuth	Elevation	Azimuth	Elevation
26	C26	-	-	-	-	182°	41°	-	-
27	C27	-	-	-	-	-	-	-	-
28	C28	-	-	-	-	-	-	322°	34°
29	C29	239°	2°	-	-	-	-	-	-
30	C30	189°	9°	41°	19°	-	-	-	-
31	C31	-	-	-	-	-	-	-	-
32	C32	100°	41°	-	-	-	-	-	-
33	C33	-	-	-	-	-	-	-	-
34	C34	-	-	-	-	-	-	-	-
35	C35	-	-	-	-	-	-	-	-
36	C36	-	-	54°	37°	-	-	-	-
37	C37	-	-	-	-	-	-	-	-
38	C38	-	-	-	-	-	-	-	-

While GPS satellites visibilities at local time (LT) over Bangkok on November 8th, 2023, shown in Table 1, there are 38 GPS satellites in the satellite number preceded by a letter indicating "G". There are 38 GPS satellites that are visibility on sky plot excluding G1, G33, G34, G35, G36, G37, and C38. There are G2, G16, G21, and G31 that can be received at sunrise and noon. There are G3, G9, G14, G17, and G30 which can be received at noon and sunset. There are G5, G11, G12, G20, and G24 which can be received at sunset and midnight. There are G10, G23, G25, and G29 which can be received at sunrise and midnight. Other that can be received for one periods of time as shown in Table 2.

Table 2 GPS satellites visibilities over Bangkok on November 8th, 2023.

No.	Time (LT)	06:00		12:00		18:00		00:00	
	Satellite	Azimuth	Elevation	Azimuth	Elevation	Azimuth	Elevation	Azimuth	Elevation
1	G1	-	-	-	-	-	-	-	-
2	G2	281°	13°	134°	38°	-	-	-	-
3	G3	-	-	180°	7°	36°	2°	-	-
4	G4	-	-	194°	51°	-	-	-	-
5	G5	-	-	-	-	207°	8°	38°	22°
6	G6	-	-	-	-	339°	55°	-	-
7	G7	-	-	331°	27°	-	-	-	-
8	G8	-	-	17°	60°	-	-	-	-
9	G9	-	-	256°	55°	110°	19°	-	-
10	G10	134°	60°	-	-	-	-	268°	0°
11	G11	-	-	-	-	280°	46°	112°	15°
12	G12	-	-	-	-	324°	4°	173°	7°
13	G13	-	-	-	-	-	-	34°	31°
14	G14	-	-	272°	7°	142°	53°	-	-
15	G15	-	-	-	-	-	-	350°	65°
16	G16	198°	16°	51°	6°	-	-	-	-

Table 2 (continued) GPS satellites visibilities over Bangkok on November 8th, 2023.

No.	Time (LT)	06:00		12:00		18:00		00:00	
	Satellite	Azimuth	Elevation	Azimuth	Elevation	Azimuth	Elevation	Azimuth	Elevation
17	G17	-	-	217°	3°	49°	35°	-	-
18	G18	-	-	-	-	-	-	331°	23°
19	G19	-	-	-	-	18°	39°	-	-
20	G20	-	-	-	-	205°	43°	67°	5°
21	G21	272°	17°	120°	40°	-	-	-	-
22	G22	-	-	-	-	129°	74°	-	-
23	G23	142°	21°	-	-	-	-	294°	21°
24	G24	-	-	-	-	286°	12°	145°	38°
25	G25	45°	24°	-	-	-	-	208°	9°
26	G26	192°	44°	-	-	-	-	-	-
27	G27	-	-	33°	21°	-	-	-	-
28	G28	335°	50°	-	-	-	-	-	-
29	G29	102°	3°	-	-	-	-	266°	62°
30	G30	-	-	317°	2°	172°	13°	-	-
31	G31	288°	52°	119°	4°	-	-	-	-
32	G32	24°	41°	-	-	-	-	-	-
33	G33	-	-	-	-	-	-	-	-
34	G34	-	-	-	-	-	-	-	-
35	G35	-	-	-	-	-	-	-	-
36	G36	-	-	-	-	-	-	-	-
37	G37	-	-	-	-	-	-	-	-
38	G38	-	-	-	-	-	-	-	-

IV. CONCLUSION AND DISCUSSION

In conclusion, the study of the visibility of BeiDou and GPS satellites can be classified according to the methods in the sky plotting process. For classifying and pinpointing the visibility of global navigation satellites above the sky, we offer the researchers to used GNSS receivers for detecting several satellites of BeiDou and GPS satellites. In the future, the research team will collect various information to study the impact on GNSS satellite signals of the ionosphere which are caused by change in the Earth's magnetic field and the occurrence of solar activity in seasons.

In discussion, the researchers were able to identify the BeiDou and GPS satellites using a method to simulate the sky over Bangkok, Thailand. The researchers were able to determine the positions of the BeiDou and GPS satellites, in the GNSS navigation satellite system, as well as research from research studies by Li et al. (2014, pp. 72-89) and Zhang et al. (2020, pp. 1-21). BeiDou satellites can be classified into different classes. According to the visual characteristics of the appearance of satellites in the sky using GNSS seismology displayed in real time, it uses a multi-frequency receiver and is a non-geometry method to model the stochasticity of GNSS navigation systems observed with multi-frequency satellite receivers. Sky visibility analysis from GNSS receivers can detect BeiDou and GPS satellites in the sky over Bangkok, Thailand.

ACKNOWLEDGEMENT

The research team would like to thank the Institute of Geology and Geophysics, Chinese Academy of Sciences (IGGCAS) and Earthquake Observation Division (EOD), Thai Meteorological Department (TMD) for supporting BG2s GNSS receiver and sharing data. We would to thank Assistant Professor Dr.Prasert Kenpankho, Department of Engineering Education, School of Industrial Education and Technology, King Mongkut's Institute of Technology Ladkrabang, Bangkok, Thailand, for experiment and data collection throughout this research.

REFERENCES

An, X., Meng, X., & Jiang, W. (2020). Multi-constellation GNSS precise point positioning with multi-frequency raw observations and dual-frequency observations of ionospheric-free linear combination. *Satellite Navigation*, *1*(1), 1-13. doi:10.1186/s43020-020-0009-x.

Cai, C., Gao, Y., Pan, L., & Zhu, J. (2015). Precise point positioning with quad-constellations: GPS, BeiDou, GLONASS and Galileo. *Advances in Space Research*, *56*(1), 133-143. doi:10.1016/j.asr.2015.04.001.

Colagrossi, A., Prinetto, J., Silvestrini, S., & Lavagna, M. (2020). Sky visibility analysis for astrophysical data return maximization in HERMES constellation. *Journal of Astronomical Telescopes, Instruments, and Systems*, *6*(4), 1-30. doi:10.1117/1.JATIS.6.4.048001.

Dabove, P., & Pietra, V. D. (2019). Single-baseline RTK positioning using dual-frequency GNSS receivers inside smartphones. *Sensors*, *19*(19), 1-17. doi:10.3390/s19194302.

Ding, M., Chen, W., & Ding, W. (2023). Performance analysis of a normal GNSS receiver model under different types of jamming signals. *Measurement*, *214*, 1-13. doi:10.1016/j.measurement.2023.112786.

Garcez, C. C., de Lima, D. V., Miranda, R. K., Mendonça, F., da Costa, J. P. C., de Almeida, A. L., & de Sousa, R. T. Jr. (2019). Tensor-based subspace tracking for time-delay estimation in GNSS multi-antenna receivers. *Sensors*, *19*(23), 1-15. doi:10.3390/s19235076.

Geng, J., Guo, J., Chang, H., & Li, X. (2019). Toward global instantaneous decimeter-level positioning using tightly coupled multi-constellation and multi-frequency GNSS. *Journal of Geodesy, 93*, 977-991. doi:10.1007/s00190-018-1219-y.

Hamza, V., Stopar, B., & Sterle, O. (2021). Testing the performance of multi-frequency low-cost GNSS receivers and antennas. *Sensors*, *21*(6), 1-16. doi:10.3390/s21062029.

Hamza, V., Stopar, B., Ambrožič, T., Turk, G., & Sterle, O. (2020). Testing multi-frequency low-cost GNSS receivers for geodetic monitoring purposes. *Sensors*, *20*(16), 1-16. doi:10.3390/s20164375.

Hamza, V., Stopar, B., Sterle, O., & Pavlovčič-Prešeren, P. (2023). Low-cost dual-frequency GNSS receivers and antennas for surveying in urban areas. *Sensors*, *23*(5), 1-19. doi:10.3390/s23052861.

Huang, K. Y., Juang, J. C., Tsai, Y. F., & Lin, C. T. (2021). Efficient FPGA implementation of a dual-frequency GNSS receiver with robust inter-frequency aiding. *Sensors*, *21*(14), 1-20. doi:10.3390/s21144634.

Jia, X., Cheng, G., Ji, Y., Sun, X., & Wu, J. (2022). GNSS single-frequency, single-epoch attitude determination method with orthogonal constraints. *Mathematical Problems in Engineering*, *2022*, 1-9. doi:10.1155/2022/4426987.

Kenpankho, P., Chaichana, A., Trachu, K., Supnithi, P., & Hozumi, K. (2021). Real-time GPS receiver bias estimation. *Advances in Space Research*, *68*(5), 2152-2159. doi:10.1016/j.asr.2021.01.032.

Li, X., Guo, B., Lu, C., Ge, M., Wickert, J., & Schuh, H. (2014). Real-time GNSS seismology using a single receiver. *Geophysical Journal International*, *198*(1), 72-89. doi:10.1093/gji/ggu113.

Liu, T., Chen, H., Chen, Q., Jiang, W., Laurichesse, D., An, X., & Geng, T. (2021). Characteristics of phase bias from CNES and its application in multi-frequency and multi-GNSS precise point positioning with ambiguity resolution. *GPS Solutions, 25*(58), 1-13. doi:10.1007/s10291-021-01100-7.

Lu, Y.-H., & Han, J.-Y. (2020). GNSS satellite visibility analysis based on 3D spatial information in urban areas. *The International Archives of the Photogrammetry, Remote Sensing and Spatial Information Sciences*, *43*, 123-128. doi:10.5194/isprs-archives-XLIII-B4-2020-123-2020.

Mao, J., Wang, Q., Liang, Y., & Cui, T. (2021). A new simplified zenith tropospheric delay model for real-time GNSS applications. *GPS Solutions*, *25*(43), 1-12. doi:10.1007/s10291-021-01092-4.

Odolinski, R., & Teunissen, P. J. (2020). Best integer equivariant estimation: Performance analysis using real data collected by low-cost, single-and dual-frequency, multi-GNSS receivers for short-to long-baseline RTK positioning. *Journal of Geodesy*, *94*(9), 1-17. doi:10.1007/s00190-020-01423-2.

Tu, R., Zhang, P., Zhang, R., Fan, L., Han, J., Hong, J., Liu, J. & Lu, X. (2021). Precise frequency transfer model suitable for short baseline link based on GPS single-differenced observations with ambiguity resolution. *Acta Geodaetica et Geophysica*, *56*, 345-355. doi:10.1007/s40328-021-00332-w.

Wielgocka, N., Hadas, T., Kaczmarek, A., & Marut, G. (2021). Feasibility of using low-cost dual-frequency GNSS receivers for land surveying. *Sensors*, *21*(6), 1-14. doi:10.3390/s21061956.

Xu, H., Hsu, L. T., Lu, D., & Cai, B. (2020). Sky visibility estimation based on GNSS satellite visibility: An approach of GNSS-based context awareness. *GPS Solutions*, *24*(59), 1-15. doi:10.1007/s10291-020-0973-5.

Yang, C. K., & Shim, D. S. (2013). Analysis of the effect of time delay on the integrated GNSS/INS navigation systems. *TransNav: International Journal on Marine Navigation and Safety of Sea Transportation*, *7*(2), 199-204. doi:10.12716/1001.07.02.06.

Zhang, B., Hou, P., Liu, T., & Yuan, Y. (2020). A single-receiver geometry-free approach to stochastic modeling of multi-frequency GNSS observables. *Journal of Geodesy*, *94*(37), 1-21. doi;10.1007/s00190-020-01366-8.

THE STUDY OF LOW-COST ROBOTICS PLATFORM FOR BEIDOU SATELLITES NAVIGATION SYSTEM

Patiphan Sumniang*, Chinakrid Janak, and Canjie Huang
E-mail: patiphan.su@kmitl.ac.th*, 65036085@kmitl.ac.th, and 65036056@kmitl.ac.th

Received: December 17, 2023
Revised: December 24, 2023
Accepted: December 28, 2023

ABSTRACT

In this study, a low-cost robot was designed for satellite navigation to promote learning in robotics and navigation satellite systems. Robot technology has been used more widely, including robots for treating disease and patients and service robots. Agricultural robots make robots play a greater role and satellite system are also used in the navigation system with robots as well. Specifically, the BeiDou satellite system was created, constructed, and tested. The BeiDou satellite system is tailored for low-cost robot applications. It utilizes components that allow for the construction of affordable and functional robotic platforms suitable for navigation using BeiDou satellites. The essential components of the low-cost robot platform for BeiDou navigation include an Arduino Nano Central Processing Unit (CPU), motor drive unit, robot structure, sensors, BeiDou satellite receiver module, and power supply. The researchers tested a robot by runing it over distances of 50 m and 100 m at low, medium, and high speeds at Sports Center King Mongkut's Institute of Technology Ladkrabang (KMITL). Tests have shown that satellite signals passing through the ionosphere cause delays that affect the accuracy of the satellite navigation system. The successfully developed low-cost robot platform for BeiDou navigation is named GNSS low-cost robotic (G-LOC robot).

Keywords: Low-cost robotics, Robotics, Robotics platform, BeiDou, Navigation satellites

*Corresponding author E-mail: Patiphan.su@kmitl.ac.th
Department of Engineering Education, School of Industrial Education and Technology,
King Mongkut's Institute of Technology Ladkrabang, Bangkok 10520 Thailand

I. INTRODUCTION

Robotics is gaining popularity across various sectors, including industry, education, and robot competitions. In the realm of education, robotics integrates the study, design, construction, operation, and utilization of robots. Robotics is considered to enhance students' interest. Nevertheless, due to the high cost of robots, not all students have the opportunity to access robotics. In engineering and computer science, robotics constitutes an interdisciplinary field of study. It encompasses the examination, design, construction, operation, and utilization of robots. Robotics, coupled with Global Navigation Satellite System (GNSS) satellite applications, serves as a dependable guide and represents a novel approach to exploring natural dynamics, sensing, and navigation. Therefore, the continuous enhancement of the accuracy and reliability of the BeiDou satellite navigation system is crucial. The goal of integrating robotics into the BeiDou satellite navigation system is to create machines capable of aiding and assisting humans. Robotics in BeiDou satellite navigation system can function as a cognitive learning tool in the educational process. Robotics integrates aspects of electrical engineering, including computer engineering, mechanical engineering, and software engineering. The incorporation of robotics can involve students in collaborative problem-solving activities, but the high cost of technology robotics remains a significant challenge. The primary concern is that schools and students may face financial constraints when implementing robotics, and exploring low-cost robotics options could address this issue.

As the literature review, Elfasakhany et al. (2011, pp. 47-55) designed and developed a competitive low-cost robot arm with four degrees of freedom. Junior et al. (2013. pp. 1-7) constructed a low-cost and simple Arduino-based educational robotics kit. They succeeded in the development of educational robotics by using Arduino and applied the robotics in the educational kit. Plaza et al. (2016, pp. 282-289) designed and constructed a collaborative robotic educational tool based on programmable logic and Arduino. Eguchi (2016, pp. 692-699) used RoboCupJunior for promoting STEM education, 21st century skills, and technological advancement through robotics competition. Plaza et al. (2017, pp. 132-136) presented home-made robotic education, a new way to explore. Darrah et al. (2018, pp. 1-4) designed and developed a low-cost open-source robotics education platform which was useful for teachers and students in school on the minimum components in a low-cost robotics. Plaza et al. (2018, pp. 1-8) used Arduino as an educational tool to introduce robotics. Chicas et al. (2019, pp. 379-383) developed STEM competences by building low-cost technology robots. Ong and Ling (2020, pp. 467-473) constructed low-cost educational robotics car to promote STEM learning and 21st century Skills. Moreover, Rajapakshe and Hettiarachchi (2022, pp. 71-76) designed, constructed, and developed a research oriented GPS low-cost robotics platform with a novel dynamic global path planning approach.

In the literature review, Elfasakhany et al. (2011, pp. 47-55) designed and developed a competitive, low-cost robot arm with four degrees of freedom. Junior et al. (2013, pp. 1-7) constructed a low-cost and simple Arduino-based educational robotics kit, successfully applying robotics in the educational context. Plaza et al. (2016, pp. 282-289) designed a collaborative robotic educational tool based on programmable logic and Arduino. Eguchi (2016, pp. 692-699) utilized RoboCupJunior to promote STEM education, 21st century Skills, and technological advancement through robotics competition. Plaza et al. (2017, pp. 132-136) introduced homemade robotic education as a novel exploration method. Darrah et al. (2018, pp. 1-4) developed a low-cost, open-source robotics education platform, beneficial for teachers and students with minimal components in a low-cost robotics setting. Plaza et al. (2018, pp. 1-8) utilized Arduino as an educational tool for introducing robotics. Chicas et al. (2019, pp. 379-383) enhanced STEM competences by building low-cost technology robots. Ong and Ling (2020, pp. 467-473) constructed a low-cost educational robotics car to promote

STEM learning and 21st century Skills. Additionally, Rajapakshe and Hettiarachchi (2022, pp. 71-76) designed, constructed, and developed a research-oriented GPS low-cost robotics platform with a novel dynamic global path planning approach.

This research presents a study on a low-cost robotics platform for BeiDou navigation. The robotics platform primarily comprises an Arduino Nano Central Processing Unit (CPU), motor, wheel, motor drive, robotic body, tracker, BeiDou navigation sensors, and power supply. The study demonstrates the creation of a low-cost robotics platform specifically designed for BeiDou navigation, focusing on applications of low-cost robotics and the minimal components required building cost-effective robotics that can be explored.

II. METHODOLOGY

A. Platform Design

The methodology of study, the low-cost robotics platform was designed using a simple Arduino-based educational robotics kit, as indicated in Table 1. The low-cost robotics platform is referred to as G-LOC ROBOT, derived from the words "GNSS low-cost robotic". Table 1 illustrates the minimum components needed to construct a low-cost robotics platform, including CPU (Arduino Nano), motor, wheel, motor drive, robotic body, BeiDou navigation and tracking, power supply, and additional items such as nuts, switches, light bulbs, and wiring. The overall cost is notably low, amounting to only 8,150 Baht.

TABLE 1 Minimum price components to build a low-cost robot.

Components	G-LOC ROBOT	Cost (Baht)
CPU	Arduino Nano	220
Motor X 4 pcs	12 VDC 150 rpm	2,200
Wheel X 4 pcs	Wheel for car racing 3.5 inches	1,000
Motor drive X 2 pcs	H-bridge 12V 40A	1,500
Robotic body	Acrylic laser cut	800
Tracker sensor X 8 pcs	IR infared sensors	560
BeiDou navigation sensors	NEO6MV2 GPS & BeiDou module	120
Power supply X 2 pcs	Li-Po battery 11.1V 1800mAh	550
Others	Nut, Switch, Light bulb, and wiring	1,200
	Total	8,150

B. Platform Construction

The researchers designed the low-cost robotics platform for BeiDou navigation using the block diagram depicted in Figure 1. The components comprise an Arduino Nano as the CPU for digital and analog input/output, two 12 DCV motors, four 3.5-inch wheels, a motor drive, an acrylic laser-cut robotic body, infrared sensors as trackers, a BeiDou navigation receiver, an 11.1V 1800mAh Li-po battery for power supply, and additional items such as nuts, switches, light bulbs, and wiring. The G-LOC ROBOT was assembled with the minimum components to explore low-cost robotics, as the objective of this study, illustrated in Figure 2.

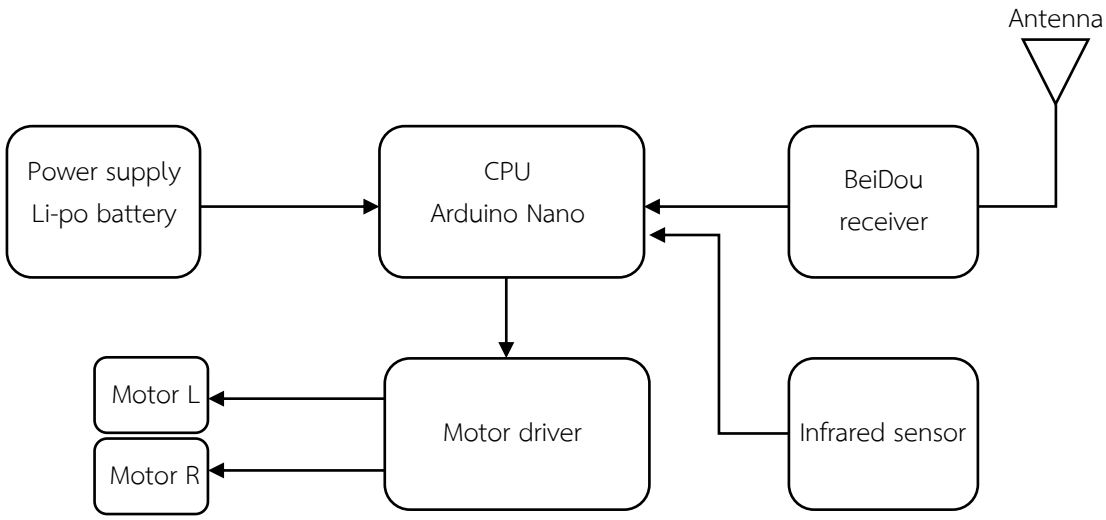

Figure 1 Block diagram of low-cost robotics platform with BeiDou navigation.

The G-LOC ROBOT was constructed with the minimum components to facilitate exploration of low-cost robotics, as depicted in Figure 2.

Figure 2 G-LOC ROBOT.

C. Platform Experiment Location

The experimental location for the G-LOC ROBOT platform for BeiDou navigation is at the soccer field, King Mongkut's Institute of Technology Ladkrabang (KMITL). There are three marked points with the same longitude 100.77177°E, for starting point with latitude 13.72976°N, 50 m point with latitude 13.73017°N, and 100 m point with latitude 13.73071°N, as shown in Figure 3.

Figure 3 The location experiments for G-LOC ROBOT.

D. Data Collection

In terms of the quality of BeiDou satellite signals, it is closely tied to the state of Earth's ionosphere propagation. The ionosphere serves as an intermediary, influencing the spread and slowing down the propagation of the signal. These changes are contingent on the ionosphere plasma density and its correlation with the sun's phase. Disruptions in the ionosphere have a direct impact on BeiDou satellites, leading to a reduction in accuracy and confidence in positioning results. Regarding ionosphere-based data collection, Reddybattula et al. (2019, p. 283) have highlighted on the positive ionospheric storms are associated with an enhancement in electron density caused by thermospheric winds, compositional changes, or the transport of ionization or electric field changes, whereas the negative storms are primarily due to compositional changes of the ionosphere (Nayak et al., 2016, pp. 7941-79601; Serafimov et al., 1982, pp. 397-399). Consequently, the data collection is segmented into four time periods: sunrise, noon, sunset, and midnight, with the G-LOC ROBOT operating at low, medium, and high speeds. The data was collected on the dates of March 29th-30th, 2023.

E. Data Analysis

BeiDou satellite signals quality is related to the state of the sun and the ionosphere propagation. The researchers make the data analysis on BeiDou navigation with the phase of the sun including sunrise, noon, sunset, and midnight. The times for data analysis are at 06.00 for sunrise time, 12.00 for noon time, 18.00 for sunset time, and 00.00 for midnight time. In addition, ionosphere is disturbed, it affects to BeiDou satellites and reduces the accuracy. Then, the researchers analyzed the BeiDou navigation with three speeds including low speed with 0.5 m/s, medium speed with 0.7 m/s, and high speed with 1 m/s.

III. RESUTLS

As indicated in Table 2, the G-LOC ROBOT during the midnight phase exhibits negative error values at both 50 m and 100 m stop points, recording -340 cm and -320 cm, respectively. During the pre-sunrise period, the low speed configuration displays the most negative value, reaching -550 cm at the 100 m stop point. At noon, the high-speed setting registers the highest value, amounting to 260 cm at both 50 m and 100 m stop points. Post-sunset times show negative error values at a 100 M distance error of -350cm for the G-LOC ROBOT. The overall trends and characteristics of errors are outlined in the presented data.

TABLE 2 The results on the experiment of low-cost robotics platform for BeiDou satellites system navigation.

Distance error (cm) Speed Time of robot test		BeiDou satellites system					
Roadway	Speed level	Midnight time 00.00 (LT)	Sunrise time 06.00 (LT)	Noon time 12.00 (LT)	Sunset time 18.00(LT)	Mean	SD
50 m	Low	-170	**-350**	**0**	**-140**	-165	143.87
	Middle	**-340**	-280	200	-110	-132.5	242.13
	High	-220	-290	**260**	-120	-92.5	245.14
	Mean	-243.33	-306.67	153.33	-123.33		
	SD.	87.37	37.86	136.14	15.28		
100 m	Low	**-320**	**-550**	200	**-350**	-255	320.05
	Middle	-140	-400	170	-240	-152.5	240.19
	High	-270	-220	**260**	-120	-87.5	239.91
	Mean	-243.33	-390.00	210.00	-236.67		
	SD.	92.92	165.23	45.83	115.04		

Table 2 shows the test results of the low-cost robot navigation by BeiDou satellites system. Test runs of 50 m and 100 m at low speed, medium speed and high speed. Perform experiments at midnight. Sunrise time, noon Sunset. The result is the distance at which the robot cannot stop in a specified position each time.

The graph of the BeiDou low-cost robotic platform satellite at a distance of 50 m as shown in **Figure 4.**

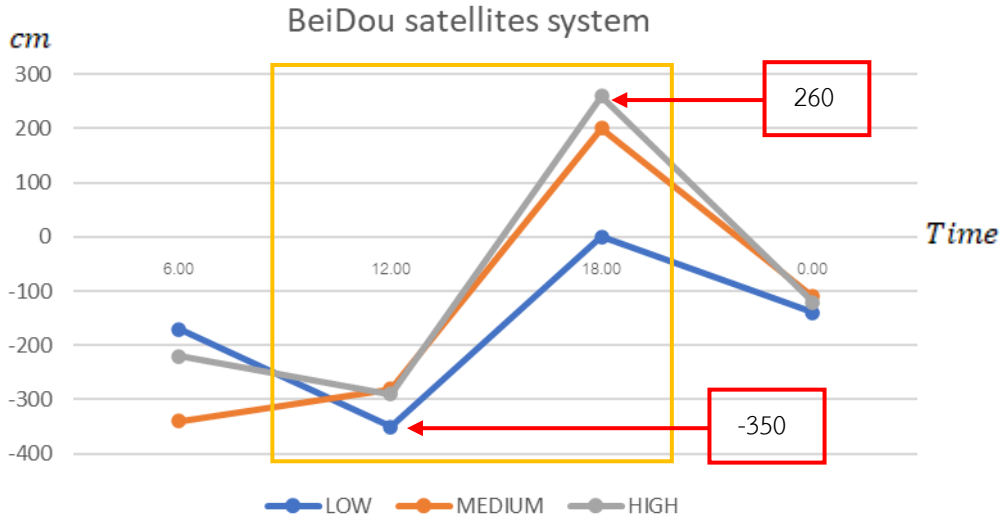

Figure 4 The result of distance of 50 m in BeiDou satellite low-cost robotic platform.

The graph in Figure 4 shows the low-cost robotic platform test error distance of 50 m with low speed, medium speed, and high speed. The results showed that the low-speed test at 12:00 noon had a maximum negative error of -350 cm and a maximum error at high speed at 6:00 p.m. by 260 cm.

The graph shows the results of a low-cost robot platform BeiDou satellites 100 m in **Figure 5.**

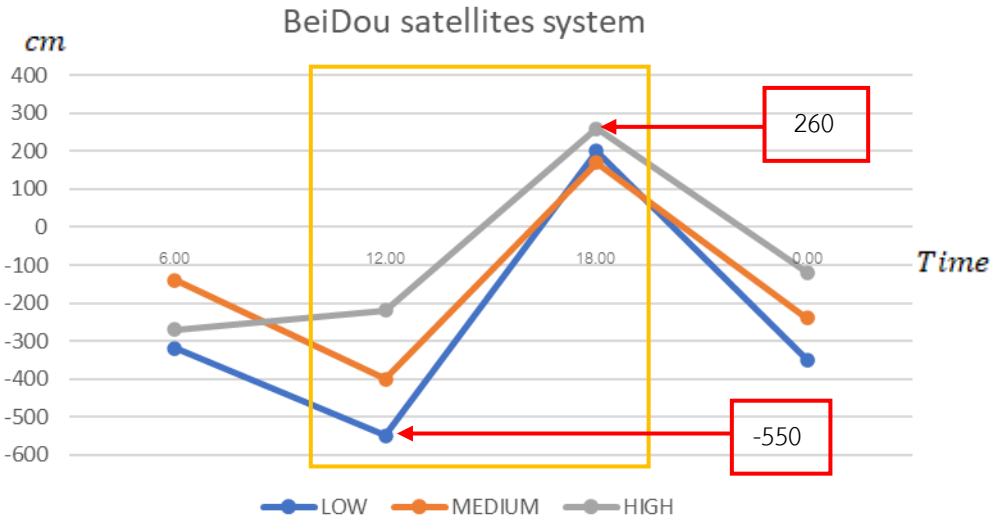

Figure 5 The result of distance of 100 m in BeiDou satellite low-cost robotic platform**.**

The graph shows the low-cost robotic platform test error distance of 100 m with test speed including low speed, medium speed, and high speed. The results showed that the low-speed test at 12:00 noon had a maximum negative error of -550 cm and a maximum error at high speed at 6:00 p.m. by 260 cm.

IV. CONCLUSION AND DISCUSSION

In the discussion, the success of the low-cost robotics platform for BeiDou navigation is highlighted, drawing parallels with previous studies such as the collaborative robotic educational tool based on programmable logic and Arduino by Plaza et al. (2016, pp. 282-289). Both the G-LOC ROBOT and the robotics platform developed by Junior et al. (2013, pp. 1-7) utilizing a low-cost and simple Arduino-based educational approach, serve as examples of effective low-cost robotic platforms. However, G-LOC ROBOT currently stands as the sole platform designed explicitly for BeiDou navigation. The experimental research introduces a novel approach to exploring robotics through home-made robotic education (Plaza et al., 2017, pp. 132-136), focusing on GPS navigation based on solar and ionospheric data. The use of Arduino as an educational tool for constructing low-cost robots is emphasized (Plaza et al., 2018, pp. 1-8) with G-LOC ROBOT serving as a dedicated platform for BeiDou navigation. Furthermore, it's noteworthy that G-LOC ROBOT was constructed at a lower cost compared to the GPS low-cost robotics designed and built by (Rajapakshe & Hettiarachchi, 2022, pp. 71-76).

In conclusion, the study successfully demonstrates the creation of a low-cost robotics platform specifically designed for BeiDou navigation. This platform is built on the principles of cost-effectiveness, utilizing minimal components that allow for exploration and experimentation. The key components of the low-cost robotics platform for BeiDou navigation include Arduino Nano, motor, wheel, motor drive, robotic body, tracker, BeiDou sensors, and power supply. The developed and effective low-cost robotic platform for BeiDou navigation is named G-LOC ROBOT. It's worth noting that the cost of G-LOC ROBOT can be further reduced by selecting alternative components while ensuring that essential capacity and performance are maintained for future use.

ACKNOWLEDGEMENT

We would like to thank to King Mongkut's Institute of Technology Ladkrabang, Bangkok, Thailand, for the experiment location at the soccer field during the experiment time. We would like to thank Assistant Professor Dr. Prasert Kenpankho from Study, Satellite, and Space Laboratory, Department of Engineering Education, King Mongkut's Institute of Technology Ladkrabang, Thailand for consulting this research.

REFERENCES

Chicas, Y., Canek, R., & Rodas, O. (2019). Developing stem competences by building low-cost technology robots: A work in progress. In A. Dutta (Ed.), *2019 IEEE Integrated STEM Education Conference (ISEC)* (pp. 379-383). IEEE.

Darrah, T., Hutchins, N., & Biswas, G. (2018). Design and development of a low-cost open-source robotics education platform. In J. Habarulema (Ed.), *50th International Symposium on Robotics (ISR 2018)* (pp. 1-4). VDE.

Eguchi, A. (2016). RoboCupJunior for promoting STEM education, 21st century skills, and technological advancement through robotics competition. *Robotics and Autonomous Systems*, *75*, 692-699.

Elfasakhany, A., Yanez, E., Baylon, K., & Salgado, R. (2011). Design and development of a competitive low-cost robot arm with four degrees of freedom. *Modern Mechanical Engineering*, *1*(2), 47-55.

Junior, L. A., Neto, O. T., Hernandez, M. F., Martins, P. S., Roger, L. L., & Guerra, F. A. (2013). A low-cost and simple arduino-based educational robotics kit. *Multidisciplinary Journals in Science and Technology, Journal of Selected Areas in Robotics and Control (JSRC), 3*(12), 1-7.

Nayak, C., Tsai, L. C., Su, S. Y., Galkin, I. A., Tan, A. T. K., Nofri, E., & Jamjareegulgarn, P. (2016). Peculiar features of the low-latitude and midlatitude ionospheric response to the St. Patrick's Day geomagnetic storm of 17 March 2015. *Journal of Geophysical Research: Space Physics*, *121*(8), 7941-7960.

Ong, S. L., & Ling, J. P. W. (2020). Low-cost educational robotics car promotes stem learning and 21 st century skills. In H. Mitsuhara, Y. Goda, Y. Ohashi, Ma. M. T. Rodrigo, J. Shen, N. Venkatarayalu, G. Wong, M. Yamada, & C.-U. Lei (Eds.), *2020 IEEE International Conference on Teaching, Assessment, and Learning for Engineering (TALE)* (pp. 467-473). IEEE.

Plaza, P., Sancristobal, E., Carro, G., & Castro, M. (2017). Home-made robotic education, a new way to explore. In C. Douligeris & M. Auer (Eds.), *2017 IEEE Global Engineering Education Conference (EDUCON)* (pp. 132-136). IEEE.

Plaza, P., Sancristobal, E., Carro, G., Blazquez, M., García-Loro, F., Martin, S., Perez, C., & Castro, M. (2018). Arduino as an educational tool to introduce robotics. In M. Lee, S. Nikolic, M. Ros, J. Shen, L. Lei, G. Wong, & N. Venkatarayalu (Eds.), *2018 IEEE International Conference on Teaching, Assessment, and Learning for Engineering (TALE)* (pp. 1-8). IEEE.

Plaza, P., Sancristobal, E., Fernandez, G., Castro, M., & Pérez, C. (2016). Collaborative robotic educational tool based on programmable logic and Arduino. In *2016 Technologies Applied to Electronics Teaching (TAEE)* (pp. 282-289). IEEE.

Rajapakshe, S., & Hettiarachchi, R. (2022). Design and development of a research oriented low cost robotics platform with a novel dynamic global path planning approach. In H. Huang & W. Pedrycz (Eds.), *8th International Conference on Control, Automation and Robotics (ICCAR 2022)* (pp. 71-76). IEEE.

Reddybattula, K. D., Panda, S. K., Ansari, K., & Peddi, V. S. R. (2019). Analysis of ionospheric TEC from GPS, GIM and global ionosphere models during moderate, strong, and extreme geomagnetic storms over Indian region. *Acta Astronautica, 161,* 283-292.

Serafimov, K. B., Arshinkov, I. S., Bochev, A. Z., Petrunova, M. H., Stanev, G. A., & Chapkanov, S. K. (1982). A measuring equipment for electric and magnetic fields in the range of the ionosphere-Magnetosphere plasma mounted aboard the “Intercosmos-Bulgaria 1300” satellite. *Acta Astronautica*, *9*(6-7), 397-399.

International Journal of Industrial Education and Technology Submission Information

1. Product of International Journal of Industrial Education and Technology (IJIET)
School of Industrial Education and Technology
King Mongkut's Institute of Technology Ladkrabang (KMTIL)

1	**Printed Schedule (Based on yearly calendar)** One issue per year as followings January – December
2	**Scopes** Publish on the academic and research articles in the term of Industrial Education and Education and Technology in specific fields follow as 1. **Teaching/Education** 2. **Engineering** 3. **Architecture** 4. **Agriculture**
3	**Who can submit and the dateline** Everyone can submit in the scopes and specific fields. Submission Dateline: Continuing submission with no dateline.
4	**Objectives** - Distributing on the advanced research and academic issues in the scopes and specific fields for all. - Reporting the advantage and valuable issues on education and research in the scopes and specific fields . - Exchanging the ideal and knowledge in education and research in the scopes and specific fields.
5	**Publication** - Printed version is published as journal to associated educational institution in public and private sector. - Online version is published on the database of TCI website. https://www.tci-thaijo.org/index.php/IJIET

2. Main Research Paper Structure

Part 1 Consists of	
1.1 Title	English should be shortly represented on the research goals
1.2 Authors	Responding author and co-authors in English giving first name and last name but no title and referring by number.
1.3 Abstract	English should be shortly focused and directly scoped on the research objective, research methodology and the research summary. It should not exceed 250 - 300 words.
1.4 Keywords	English should choose keywords related to article and at least three words.

Part 2 Contents

I. INTRODUCTION

Consists of four paragraphs.

Paragraph #1 Statement of purpose with specific information and hypothesis.

Paragraph #2 Literature reviews articles according to the article.

Paragraph #3 Literature reviews/ New ideals on research methodologies that are for the article.

Paragraph #4 Objectives are only in descriptive writing but not also no number column.

It should not exceed one and a half pages.

Part 3 Consists of	
II. METHODOLOGY	Writing methodology in detail with sub context (if need)
III. RESULTS AND DISCUSSION	Showing the results in table and/or in picture. Describing the results with understandable information. Discussing the results with literature reviews, reasons, and other matters.
IV. CONCULSION	Writing the statement and conclusion of research article.
ACKNOWLEDGEMENT	Giving the credits to others such as funding, consultant, helpers, and so on.

Part 4 References

REFERENCES

The APA reference style must be used as the requirement of International Journal of Industrial Education and Technology. The references are only referred in the research paper to be in this reference part. The APA reference style should be applied for the whole subject. The writer is to be responsibility for the correction and the copyright of referring in the research.

3. Printed Format

3. Printed format

3.1 Thai and English Research Paper

Paper setting (6-20 pages (NOT exceed 20 pages))

- Font Th SarabunPSK only
- paper size top 1 inch bottom 1 inch left 1 inch right 0.8 inch

***Please follow the Template file which can be downloaded as** .....

3.2 Titles

In Thai and English. For English, using the Upper case (18 Bold inch)

3.3 Author and Co-authors

It should be written in all righted authors. Identify the responded author with email (15 Bold inches).

3.4 Abstract and Contents

- Abstract is written in 14 bold inch and place it on the left side.

The word Abstract, only letter A is upper case and others are in 14 inches with 1 column.

- Contents are in 1 column with the headline in 16 bold inches and sub headline is in 14 bold inches. The contents are in 14 inches and given in 5 spaces.

3.5 Keywords): Fonts size 14 inches.

3.6 Figure and Table

1. Leaving 1 row before inserting the table and giving 1 row before writing the information for the table in details.

2. Uses "Table **...**" at the left corner with font 12 bold inch.

3. Table name is in font 12 inches and if the table detail is longer than 1 row, it should be started with new row by the same starting column.

4. Using only in column table as opened the left and right alignments.

Table 1 (Table name is in 12 inches.)

Title (12 bold inch.)	**Title**	**Title**	**Title**	**Title**
Content (12 inches.)	Content	Content	Content	Content
Content	Content	Content	Content	Content

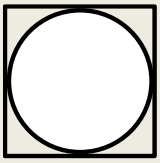

Figure 1 **.....** (Font is in 13 inches with in center column)

3.7 Discussion part in 16 inches.

At left column for contents. For first row in each paragraph, it has to give 4 word-spaces (font in 14 inches.)

3.8 Conclusion part in 16 inches.

At left column for contents. For first row in each paragraph, it has to give 4 word-spaces (font in 14 inches.)

3.9 Acknowledgement in 16 inches. Without putting number in front of topic (Font in 14 inches.)
No needs to put the number for this content (font in 14 inches.)

3.10 References title font in 16 inches.
(Content font is in 14 inches.)

3.11 $\bar{X}$ and Table Format

- Create your own table in column and Do Not Copy table form from other file sources.
- Use $\bar{X}$ as only in this following size $\bar{X}$ (S.D.) ($\bar{X} \geq 3.50$) ($\bar{X} = 4.51$).

3.12 Sub title format (Example)

1. Title (16 bold inches)
1.1 Sub title (6 word-spaces in 14 font inches.)
1.1.1 Second sub title (alignment as the first world of sub title in 14 font inches.)
1.1.1.1 Third sub title
(1) sub title of 1.1.1.1
(1.1) sub title of (1)

Paper preparing and submitting for International Journal of Industrial Education and Technology

For correction, perfection, and time saving, paper submission for publishing in International Journal of Industrial Education and Technology is needed to follow as this guideline.

1.1 Printed and typed in A4 paper size for 6-11 pages with one column style. By using Microsoft Word, it is highly recommended the word processing software that fits in the International Journal of Industrial Education and Technology format guideline according to our time saving for paper proof and publishing.

1.2 The original or submitted paper must be only formatted as the Journal of Industrial Education printed format. **If NOT follow as directions, the author is informed and the paper will NOT be stepped any forward.**

1.3 Paper is needed to be clear in contents and pictures.

1.4 Paper is Not published or Not printed in any sources such as journal, conferences, so on.

1.5 The author is fully responsibility to prove the correction of any requirement of Journal of Industrial Education format.

1.6 Typing or writing journal application form and attach transfer receipt.

1.7 Filling and signing on form to submit industrial education journal article. The first name is the author's name, then the second to sixth are advisor names and so on.

1.8 Preparing and submitting paper is noted as forms at https://www.tci-thaijo.org/index.php/IJIET.
SCAN PDF FILE AND MICROSOFT WORD(.doc. or .docx.) to database and naming the files separately.

1.9 Competely fill out the member form of Journal of Industrial Education.
Scan it, attach it to ThaiJo system, and post confirmed mail.

1.10 Competely transferred the member fee for International Journal of Industrial Education and Technology.

Scan it, attach it to ThaiJo system, and post confirmed mail.

1.11 Competely fill out the submitting form for Journal of Industrial Education with requirement in 1.6.
Scan it, attach it to ThaiJo system, and post confirmed mail.

1.12 For the preparing and submitting paper, please see the direction and guideline of International Journal of Industrial Education and Technology at URL: https://www.tci-thaijo.org/index.php/IJIET (Guideline is also in website).

Contact us:

Mrs. Jantanee Supsaendee Assistant Editor
Mobile phone number 086 349 6020 (office hours)
Telephone number 0 2329 8000 EXIT 3720 (office hours)
Fax number 0 2329 8435 (office hours)

Address:

Academic Services for Social Affairs
(International Journal of Industrial Education and Technology, KMITL.)
School of Industrial Education and Technology, King Mongkut's Institute of Technology Ladkrabang
No. 1, Soi Chalongkrung 1, Ladkrabang subdistrict, Ladkrabang district, Bangkok 10520

4. Paper Submission is ONLY on ThaiJo

If the author DOES NOT follow as the direction, paper will NOT BE considerred!

********Link....Important needs********

① IJIET Member form: https://drive.google.com/file/d/1Z4b8yuemMYTwpsEnnDzzlHLkPADurUGx/view
② Paper submitting form: https://drive.google.com/file/d/1ZMWINlA5BjFiOqHHvP2KOZwbngA6c5Zq/view
③ Template **paper format**: https://drive.google.com/file/d/1J6955l2yCkoQRWuDAueun6C-RPBWcU5V/view

******Contact us if you have any questions******

E-mail : Journal.ided@kmitl.ac.th

IJIET

INTERNATIONAL JOURNAL OF INDUSTRIAL EDUCATION AND TECHNOLOGY

www.siet.kmitl.ac.th | www.tci-thaijo.org/index.php/IJIET
journal.ided@kmitl.ac.th 02 329 8000 ext. 3723
1 Chalongkrung Rd. Ladkrabang, Bangkok Thailand 10520